Naked singularities and other features of self-similar general-relativistic gravitational collapse

Amos Ori and Tsvi Piran*
Racah Institute for Physics, The Hebrew University, Jerusalem 91904, Israel
(Received 29 June 1989)

Self-similar solutions are commonly used to describe Newtonian gravitational collapse. We examine, here, the structure of general-relativistic spherical collapse solutions for a perfect fluid with a barotropic equation of state. We find that these solutions are quite different from the homogeneous Oppenheimer-Snyder dust collapse solution on which our intuition is so heavily based. The most amazing feature that we find is the generic appearance of naked singularities in these solutions.

I. INTRODUCTION

One of the main difficulties in the study of gravitational collapse is that only a few exact solutions to Einstein equations are known which are relevant to gravitational collapse with reasonable matter. New collapse solutions are therefore very useful, even if they are simplified ones. Today, 50 years after Oppenheimer and Synder[1] proposed the spherical homogeneous dust collapse model, most of our knowledge and intuition about gravitational collapse is still based on that model. Obviously, this model is oversimplified, because we believe that gravitational collapse begins from a very inhomogeneous initial state, with a strong centrally peaked density profile. Nevertheless, despite its simplicity it describes well the formation of the horizon, and the evolution of the central, spacelike singularity. In a sense, this simplified model, in which the singularity is formed inside a black hole, gave the basic motivation to the concept of cosmic censorship. According to the cosmic censorship conjecture,[2] the singularities that appear in a gravitational collapse (in an asymptotically flat universe) are always surrounded by an event horizon. Moreover, according to the strong version of cosmic censorship, such singularities are not even locally naked (that is, no timelike or null curves can emerge from these singularities).

A significant improvement to the model of Oppenheimer and Snyder is obtained by the application of the Tolman-Bondi solution for inhomogeneous spherical dust collapse (see, e.g., Ref. 3). This model can exhibit two kinds of naked singularities: a shell-crossing singularity[4] and a shell-focusing singularity.[5-7] These kinds of naked singularity are generic for spherical dust collapse, and with proper choice of initial data they are globally naked.

The main deficiency of the Tolman-Bondi model is that it neglects the pressure, which is likely to diverge at these singularities (where the density diverges). One can expect that for a reasonable equation of state the pressure gradients will prevent the formation of shell-crossing singularities. However, the situation is not so clear concerning the shell-focusing singularities. Unfortunately, there are only a few known collapse solutions with an equation of state that is reasonable and well determined (there are several solutions with "formal" equations of state, that is, one postulates the metric coefficient and then calculates both the pressure and density via Einstein equations). This lack of collapse solutions makes it difficult to test the cosmic censorship hypothesis, as well as other ideas concerning gravitational collapse.

It is well known that the Einstein equations admit self-similar solutions. Self-similar space-times are defined by the existence of a homothetic Killing vector. Along each integral curve of that vector field all the points are similar to each other, apart from a scale factor that evolves linearly with the proper length along the integral curve in question. Self-similar space-times were studied by several authors.[8-11] So far, they have been used mainly in the cosmological context.[9,10,12-14] It is the purpose of this paper to use self-similarity to model spherical-symmetric gravitational collapse of compact objects with reasonable equation of state.[15,16] This attempt is not trivial, because the definition of self-similarity is kinematic (the existence of a homothetic Killing field), while the natural formulation of a collapse problem is an an initial-value problem (with an equation of state defined *a priori*). It was shown, however,[9,13] that a $p=k\rho$ equation of state is compatible with self-similarity (where p is the pressure, ρ is the density, and k is a constant). For this equation of state, if the initial profiles of density, velocity, and gravitational potential satisfy some ordinary differential equations (the equations of self-similarity, to be described in Sec. II), the system will evolve in a self-similar manner. $p=k\rho$ is the only barotropic equation of state compatible with self-similarity. This equation of state, even if simplified, is nevertheless physically consistent in the whole range $0\le k\le 1$. In the case $k=\frac{1}{3}$ it is just the equation of state of "radiation." The special case $k=0$ coincides with the dust case. In Sec. II A we will further discuss the physical interpretation of that equation of state for arbitrary k values.

The main difficulty that appears when one tries to employ self-similarity to describe gravitational collapse is the asymptotic behavior at infinity. In the context of gravitational collapse of compact objects we would generally like the space-time to be asymptotically flat. On the contrary, self-similar solutions are not asymptotically

flat. For instance, in a fully self-similar solution the mass of the collapsing "object" is infinite. In order to model the collapse of a finite-mass object, it is necessary therefore to match a self-similar interior to a Schwarzschild exterior. In Sec. VI we perform such a matching via an intermediate region. We show that if the matching (which can be done as smoothly as desired) is sufficiently far from the center, the central region will not be affected by this matching, and it will evolve in a self-similar manner, until a sufficiently late stage of the collapse.

With self-similarity, Einstein equations are reduced to a set of ordinary differential equations. This enables one to solve them numerically in a simple and reliable manner. It is also relatively easy to study the asymptotic behavior of these equations near the critical points that exist in the various solutions. Because of its simplicity, one can use self-similar collapse models to test various ideas in the theory of gravitational collapse. Our main attention in this paper is devoted to the cosmic censorship hypothesis. In a spherical self-similar space-time it is easy to solve the equation of motion for radial null geodesics, and this enables us to study the causal structure of the space-time. In Sec. V we show that in a significant part of the space of self-similar solutions there is a globally naked central singularity from which null geodesics emerge to infinity. To our best knowledge this is the only known counterexample to cosmic censorship for a perfect fluid with pressure. In this respect, this is probably the strongest known counterexample to cosmic censorship.

We point out that this counterexample is not regarded as a total contradiction to cosmic censorship. The formulation of Penrose[2] to this conjecture deals with *stable* space-times with naked singularities, and it is not yet known whether the self-similar solutions discussed in this paper are stable. It is well known that in several examples of space-time with naked singularities [the maximum extensions of Reissner-Nordström, Kerr and Kerr-Newman, Taub-Newman-Unti-Tamburino (NUT), etc., space-times] the Cauchy horizon is unstable to the formation of a "blue sheet"—a null hypersurface on which the blueshift diverges (see Ref. 17 and references there). It is therefore important to note that in the naked-singular self-similar solutions that we discuss in this paper the Cauchy horizon is *not* subject to a blue-sheet instability.[18] It is still possible, however, that other modes of instability exist in these solutions. In addition to the Cauchy horizon, there exists in the self-similar solutions another characteristic hypersurface (the "sonic point"; see Sec. VII), associated with sound waves. One might expect that like the blue-sheet instability, some sort of hydrodynamic instability will be associated with this hypersurface. Recently we have studied the stability of the equivalent Newtonian self-similar collapse solutions. We have found[19] that most of these solutions are subject to such an instability (the "kink instability"; see Sec. III A). There exists, however, a discrete set of self-similar solutions which are stable to this mode. We expect, but have not verified, that the same situation occurs in the relativistic self-similar solutions.

Newman[20] proposed an alternative formulation to the cosmic censorship hypothesis, in which the requirement for stability is replaced by the requirement that the naked singularity is strong (in the sense defined by Tipler *et al.*[17]). He has shown that both the shell-focusing dust naked singularities and the shell-crossing dust naked singularities[4] that was found by Eardley and Smarr[5] and by Christodoulou[7] are not strong. On the other hand, in some of the Vaidya solutions[21] there are null geodesics that emerge out of a strong naked singularity to infinity. But ingoing null geodesics that reach this singularity do not end in a strong singularity. He suggests, therefore, that nature avoids naked singularities in which both incoming and outgoing null geodesics end in a strong singularity. This has motivated us to study the strength of the singularity in the naked-singular self-similar solutions. In Sec. V we show that for both incoming and outgoing null geodesics the naked singularity is strong. This contradicts Newman's formulation for the cosmic censorship hypothesis. Lake[22] and Lake and Waugh[18] have shown, independently, that the Cauchy horizon in our self-similar naked-singular solutions emerges from a strong singularity. The analysis here is more general and includes both outgoing and ingoing null geodesics.

Self-similar models are widely used to describe Newtonian collapse, of matter with either isothermal[23–28] or polytropic[29] equations of state. From the point of view of local physics, the equation of state $p=k\rho$ can be associated with both types of equations of state (see Sec. II A). However, mathematically the relativistic self-similar model is related to the isothermal model. The latter is, in fact, a limiting case of the relativistic self-similar solution. We discuss the isothermal Newtonian self-similar model and its connection to the relativistic model in Sec. III.

In Sec. II we present the basic equations and the basic formal structure of the self-similar solutions in both Schwarzschild and comoving coordinates. Other coordinates (such as double-null coordinates) are also useful, but we will not use them here. Section III describes briefly the equivalent Newtonian model and its connection to the relativistic model. In Sec. IV we discuss the overall physical structure of relativistic self-similar solutions—the occurrence of singularities, the existence of regular center, sonic point, apparent horizons, etc., and the asymptotic behavior at infinity.

Section V is devoted to analysis of null geodesics and causal structures. We first show the existence of a few especially simple null geodesics (ingoing and/or outgoing), which play a central role in the analysis of null geodesics. We then explore the causal structure of the self-similar solutions, and find out that there are two kinds of solutions: with and without naked singularity. For naked-singular solutions we show the existence of one nonradial simple null geodesic that spiral out infinite times on its way from the naked singularity to null infinity. We calculate the time dependence of the redshift of light emitted from a source located at the center, and find out that this redshift diverges at the moment that the naked singularity appears. We study the strength of the naked singularity for four simple null geodesics: one ingoing (the "anti-Cauchy" horizon) and three outgoing: the event and Cauchy horizons, and the simple spiral

geodesic. We find out that this singularity is strong for all of these null geodesics.

In Sec. VI we discuss the matching of self-similar interior to an asymptotically flat exterior by means of a cutoff. In Sec. VII we discuss the properties of the "sonic point," a critical point that exists in all the self-similar solutions, and its implication on the structure of space of solutions. In Sec. VIII we briefly discuss the special case $k=0$, the self-similar dust solutions.

II. BASIC EQUATIONS

A. Spherical self-similar space-times

Self-similarity is defined invariantly by the existence of a homothetic Killing vector field.[9-11] In specific coordinate systems, self-similarity is manifested by a simple scaling relation for the metric functions. For instance, a spherical space-time is self-similar if there exist a radial area coordinate r and an orthogonal time coordinate t for which the metric functions satisfy

$$\begin{aligned} &g_{tt}(ct,cr)=g_{tt}(t,r)\ , \\ &g_{rr}(ct,cr)=g_{rr}(t,r)\ , \end{aligned} \tag{2.1}$$

for every $c>0$ (see Sec. II B). A similar relation exists for comoving coordinates (see Sec. II C) as well as other coordinate systems.

If the matter field is a perfect fluid one can verify that the only barotropic equation of state which is consistent with Eq. (2.1) is of the form

$$p=k\rho\ , \tag{2.2}$$

where ρ is the total energy density, p is the pressure, and k a constant.

Equation (2.2) can be viewed as either (1) an equation of state of isothermal gas (when adiabatic heating or cooling is neglected, and when the internal energy is negligible compared with the rest mass) or (2) an extreme relativistic limit of an adiabatic equation of state

$$p=aN^{k+1}\ . \tag{2.3}$$

When the rest mass of the particles is negligible relative to the internal energy we obtain

$$\rho=\frac{a}{k}N^{1+k}\ , \tag{2.4}$$

which leads to Eq. (2.2).

In the context of gravitational collapse and singularity formation, which we are interested in, it is natural to adopt the second interpretation.

B. Representation in Schwarzschild coordinates

We define "Schwarzschild-like" coordinates (r,t) as

$$ds^2=-e^{\nu}dt^2+e^{\lambda}dr^2+r^2d\Omega^2\ , \tag{2.5}$$

where $d\Omega^2=d\theta^2+\sin^2\theta\,d^2\phi$. There are four hydrodynamic variables ρ,p and u^t,u^r the components of the four-velocity. ρ and p are related by Eq. (2.2) while u^t and u^r by

$$-e^{\nu}u^{t2}+e^{\lambda}u^{r2}=-1 \tag{2.6}$$

with four independent functions ν, λ, ρ, and u^r. In a self-similar solution we can express these functions as

$$\begin{aligned} &\rho\equiv\frac{D(x)}{4\pi r^2},\quad \lambda=\lambda(x)\ , \\ &\nu=\nu(x)\ , \\ &u^r=u^r(x),\quad u^t=u^t(x)\ , \end{aligned} \tag{2.7}$$

where

$$x\equiv\frac{r}{t} \tag{2.8}$$

is the self-similarity variable. The Einstein spherical self-similar equations in these coordinates become

$$T^0_0:\ 2D(u_tu^t-ku_ru^r)=(1-e^{-\lambda})+xe^{-\lambda}\lambda'\ , \tag{2.9a}$$

$$T^1_1:\ 2D(u_ru^r-ku_tu^t)=(1-e^{-\lambda})-xe^{-\lambda}\nu'\ , \tag{2.9b}$$

$$T^0_1:\ 2(k+1)Du^ru_t=x^2e^{-\lambda}\lambda'\ , \tag{2.9c}$$

$$u^{\alpha}T_{\alpha}{}^{\beta}{}_{;\beta}:\ -k\left[u^r\left[D'-\frac{2D}{x}\right]-xu^tD'\right]+(k+1)e^{-(\lambda+\nu)/2}[(De^{(\nu+\lambda)/2}u^r)'-x(De^{(\lambda+\nu)/2}u^t)']=0\ , \tag{2.9d}$$

where a prime means a derivative with respect to x.

The line element [Eq. (2.5)] is invariant under a transformation of the form $t\to\hat{t}(t)$, $\nu\to\hat{\nu}$. However, Eq. (2.7) and the field equations (2.9a)–(2.9d) are not invariant under this transformation. These equations and the subsequent discussion are invariant to a transformation of the form $t\to\hat{t}=at$. Clearly this transformation amounts just to a linear rescaling of x.

We shall call the particular coordinates, for which Eqs. (2.5), (2.7), and (2.9a)–(2.9d) are valid "self-similar Schwarzschild (SSS) coordinates." One may also use the "ordinary Schwarzschild coordinates," for which the metric is given by Eq. (2.5) and $\lim_{r\to\infty}\nu=\lim_{r\to\infty}\lambda=0$. A full self-similar space-time is not asymptotically flat hence these coordinates are irrelevant for it. However, we introduce later a cutoff which enables us to have asymptotically flat solutions and the ordinary Schwarzschild coordinates are applicable in describing these solutions.

The mass $m(r,t)$ is defined by $e^{-\lambda}\equiv1-2m/r$. We

define $\mathcal{M}$ as

$$\mathcal{M}(x)\equiv\frac{m}{r}=\frac{1}{2}(1-e^{-\lambda}) . \tag{2.10}$$

We can rewrite now (2.9a)–(2.9c) as

$$x\mathcal{M}'=D[1-(k+1)u_r u^r]-\mathcal{M} , \tag{2.9a'}$$

$$-\tfrac{1}{2}x\nu' e^{-\lambda}=D[1-(k+1)u_t u^t]-\mathcal{M} , \tag{2.9b'}$$

$$x\mathcal{M}'=(k+1)\frac{D}{x}e^{\lambda}u^r u_t . \tag{2.9c'}$$

Equations (2.9a') and (2.9c') yield an algebraic expression for u^t:

$$u_t=x\frac{D[1-(k+1)u_r u^r]-\mathcal{M}}{(k+1)De^{\lambda}u^{r2}}\equiv xQ . \tag{2.11}$$

Using Eqs. (2.6) and (2.11) we find

$$e^{\nu}=\frac{Q^2}{1+e^{\lambda}u^{r2}}x^2 \tag{2.12}$$

and

$$u^t=\frac{1+e^{\lambda}u^{r2}}{Qx} , \tag{2.13}$$

and we are left only with three independent functions: D, u^r, and $\mathcal{M}$.

In Appendix A we show that we can get rid of x from this system of equations and reduce the number of independent functions to two. We can use one of the independent functions, say λ, as an independent variable and express u^r and D as function of λ. A given point (λ,D,u^r) can be assigned to an arbitrary value of x. This freedom corresponds to the transformation $t\to\hat{t}=at$ which leads to $x\to\hat{x}=x/a$. Such a transformation leaves u^r, D, and λ unchanged.

In solutions describing spherical collapse we require, that at least initially, the solution is regular at the origin. (We will see later that a singularity forms at the origin at $t=0$.) We call the regular world line ($t<0$, $r=0$) the "regular center" and we denote it by 0^-. With a regular center we impose two boundary conditions at the origin:

$$u^r(0)=0, \quad u^t(0)=1 . \tag{2.14}$$

The first condition corresponds to the requirement that the matter flow is regular at the center. The second condition is just a convenient scaling of the time coordinate which is set to be equal to the proper time of a particle at rest at the regular center. This condition fixes t and x and with it we can no longer transform $t\to\hat{t}=at$.

We expand Eqs. (2.9a)–(2.9c) to second order in x near 0^-. We find that the behavior near the origin is characterized by $D_0\equiv\lim Dx^{-2}$:

$$x^{-2}D=D_0+D_0\left[\frac{2}{3(k+1)}+\frac{3k+1}{6k}\left[\frac{2}{3(k+1)}\right]\right]x^2 +O(x^4) , \tag{2.15a}$$

$$u^r=\frac{2}{3(k+1)}x+O(x^3) , \tag{2.15b}$$

$$u^t=1+\left[\frac{2}{9(k+1)}-\frac{D_0(3k+1)}{6}\right]x^2+O(x^4) , \tag{2.15c}$$

$$\lambda=\tfrac{2}{3}D_0x^2+O(x^3) , \tag{2.15d}$$

$$\nu=D_0(k+\tfrac{1}{3})x^2+O(x^4) . \tag{2.15e}$$

We see that for a given k the solutions with a regular center form a one-parameter family of solutions. In Sec. VIII we show that the solution must have a critical point and beyond it the family of regular solutions is two dimensional.

C. Comoving coordinates

We define comoving coordinates (T,R) by requiring that in these coordinates

$$u^{\mu}=u^T\delta^{\mu}_T . \tag{2.16}$$

The comoving line element is

$$ds^2=-e^{\Psi}dT^2+e^{\Lambda}dR^2+r^2d\Omega^2 . \tag{2.17}$$

The normalization condition $u_{\mu}u^{\mu}=-1$ yields, therefore,

$$u^T=e^{-\Psi/2} . \tag{2.18}$$

We define a comoving similarity variable $y=R/T$ and write the hydrodynamic and metric functions as

$$\rho(R,T)=\frac{D(y)}{4\pi r^2}, \quad \Psi(R,T)=\Psi(y) , \quad \Lambda(R,T)=\Lambda(y), \quad r(R,T)=\tilde{r}(y)T . \tag{2.19}$$

As in the Schwarzschild coordinates, the comoving condition [Eqs. (2.16) and (2.18)] and the form of the line element [Eq. (2.17)] are invariant under a transformation of the form: $T\to\hat{T}(T)$, $R\to\hat{R}(R)$. However, the self-similar structure [Eq. (2.19)] is not invariant under this transformation unless they are linear, i.e., $\hat{T}=aT$ and $\hat{R}=bR$.

We will call comoving coordinates for which (2.19) holds "self-similar comoving (SSC) coordinates."

Substitution of the self-similarity condition [Eq. (2.19)] in the comoving spherical Einstein equations yields

$$T^1_0: \quad -2y\tilde{r}''-\Psi'(\tilde{r}-y\tilde{r}')+y\Lambda'\tilde{r}'=0 , \tag{2.20a}$$

$$T^0_0: \quad 1+e^{-\Psi}(\tilde{r}-y\tilde{r}')(\tilde{r}-y\tilde{r}'-y\tilde{r}\Lambda') -e^{\Lambda}(2\tilde{r}\tilde{r}''+\tilde{r}'^2-\tilde{r}\tilde{r}'\Lambda')=0 , \tag{2.20b}$$

$$T^{\mu}_{1;\mu}: \quad \Psi'=-\frac{2k}{k+1}\frac{\tilde{D}'}{\tilde{D}} , \tag{2.20c}$$

$$T^{\mu}_{0;\mu}: \quad -\Lambda'=\frac{2}{k+1}\left[\frac{\tilde{D}'}{\tilde{D}}+\frac{2}{y}\right]+4\left[\frac{\tilde{r}'}{\tilde{r}}-\frac{1}{y}\right] , \tag{2.20d}$$

where we have defined $\tilde{D}\equiv D/\tilde{r}^2=4\pi\rho T^2$, and a prime now means a derivative with respect to Eqs. (2.20c) and (2.20d) can be integrated immediately to yield

$$\Psi=-\frac{2k}{k+1}\ln\tilde{D}+a_{\Psi} , \tag{2.21a}$$

$$\Lambda=-\frac{2}{k+1}(\ln\tilde{D}+2\ln y)-4(\ln\tilde{r}-\ln y)+a_{\Lambda} , \tag{2.21b}$$

a_Λ and a_Ψ are arbitrary constants which corresponds to the freedom to perform the linear coordinate transformations $T \to aT$, $R \to bR$. A coordinate choice $e^\Psi = 1$ at the regular center will fix a_Ψ. With this choice $T = t$ at the regular center. Another arbitrary coordinate choice will fix a_Λ and the scaling of R.

Substitution of Eqs. (2.21a) and (2.21b) in (2.20a) and (2.20b) yields a closed system of two ordinary differential equations for $\tilde{D}$ and $\tilde{r}$. The system is of first order for $\tilde{D}$ and of second order for $\tilde{r}$. As in the SSS case there are, in fact, only 2 physical degrees of freedom in the solution.

D. Transformation from SSC to SSS coordinates

Self-similarity is an intrinsic geometrical property of the space-time. Hence if we can express a solution in SSC coordinates there exist corresponding SSS coordinates. We show here that a coordinate transformation between these two systems exists. The diagonal form of Eq. (2.5) yields

$$0 = g^{tr} = e^{-\Lambda}\left[\frac{\partial t}{\partial R}\right]\left[\frac{\partial r}{\partial R}\right] - e^{\Psi}\left[\frac{\partial t}{\partial T}\right]\left[\frac{\partial r}{\partial T}\right] . \tag{2.22}$$

We define $\tilde{t} = t/T$ and look for a solution of Eq. (2.22) of the form

$$\tilde{t}(R,T) = \tilde{t}(y) . \tag{2.23}$$

We obtain a first-order differential equation

$$e^{-\Lambda}\tilde{t}'\tilde{r}' - e^{-\Psi}(\tilde{t} - y\tilde{t}')(\tilde{r} - y\tilde{r}') = 0 \tag{2.24}$$

that defines $\tilde{t}(y)$ up to an integration constant. The latter is fixed by the requirement that at the regular center $T = t$, hence $\tilde{t}(0) = 1$. We define now the SSS similarity variable

$$x = r/t = \tilde{r}/\tilde{t} = x(y) . \tag{2.25}$$

The world lines $x = \text{const}$, which correspond to $y = \text{const}'$, are the invariant curves of the homothetic Killing vector that exists in the space-time. Generally the inverse function, $y = y(x)$ exists, and we can transfer all functions of y to functions of x. The rest of the metric functions are

$$e^{-\lambda} = e^{-\Lambda}\tilde{r}'^2 e^{-\Psi}(\tilde{r} - y\tilde{r}')^2 \tag{2.26a}$$

and

$$e^{-\nu} = e^{-\Psi}(\tilde{t} - y\tilde{r}')^2 - e^{-\Lambda}\tilde{t}'^2 . \tag{2.26b}$$

The velocities are

$$u^r = e^{-\Psi/2}(\tilde{r} - y\tilde{r}') , \tag{2.27a}$$

$$u^t = e^{-\Psi/2}(\tilde{t} - y\tilde{t}') . \tag{2.27b}$$

D is the same in both coordinate systems. The right-hand side (RHS) of Eqs. (2.26a) and (2.26b) and Eqs. (2.27a) and (2.27b) is a function of y only. Using Eq. (2.25), one finds that the metric functions, the velocities, and D are functions of x.

The regular center is located, in the SSC coordinates, in $R_{ce} = 0$. This is the only choice which is consistent with self-similarity. ($\tilde{r}$ must vanish at the center hence this must be a self-similar world line and the only consistent choice $y_{ce} = 0$ leads to $R_{ce} = 0$.)

For a given finite y value, R, r, and t are proportional to T and all three vanish when $T = 0$. Hence $(R,T) = (0,0)$ corresponds to $(r,t) = (0,0)$. We will denote this point as the origin or simply by (0,0).

E. The singularities

The point (0,0) is singular in every self-similar solution. To see this we consider the density at the regular center:

$$\rho(T,0) = \frac{\tilde{D}(0)}{4\pi T^2} \tag{2.28}$$

and the density diverges at $T = 0$. The density diverges also when we approach the origin (0,0) along any self-similarity line of the form $y = y_0$:

$$\rho(T, y_0 T) = \frac{\tilde{D}(y_0)}{4\pi T^2} . \tag{2.29}$$

The density at $T = 0$ for $R \neq 0$ is finite since

$$\lim_{T\to 0} \rho(T, R \neq 0) = \lim_{T\to 0} \frac{D_\infty}{4\pi r(R,T)^2} , \tag{2.30}$$

where $D_\infty \equiv \lim_{y\to\infty} D$ (Ref. 30).

The singularity at the origin follows directly from the self-similar structure of the solution [Eqs. (2.7) and (2.19)] and it does not reflect any singularity of the solutions of Eqs (2.9a) and (2.9d) or (2.20a) and (2.20d). *This singularity is the one that can be seen from infinity in some solutions.* The divergence of the density in this singularity results also in a divergence of the curvature scalars there. In general in a perfect fluid the divergence of the density leads, necessarily, to divergence of the scalar $R^\beta_\alpha R^\alpha_\beta$ which satisfies $R^\beta_\alpha R^\alpha_\beta = \rho^2 + 3p^2$. The Ricci scalar $R^\alpha_\alpha = \rho - 3p$ divergences also if $k \neq \frac{1}{3}$.

In the solutions that we discuss in this paper, "black-hole-type" solutions, there is a Cauchy horizon emerging from the singularity at (0,0) (see Sec. V) when this singularity is naked. In these cases we continue the solution analytically across the Cauchy horizon. The following discussion of the structure of the space-time beyond the Cauchy horizon depends on this continuation. When the singularity is not naked the evolution that follows the formation of the singularity at the origin follows directly from the initial data. In both cases the singularity that forms at (0,0) acquires mass at a rate proportional to T (see Fig. 8 and the discussion in Sec. IV D). At $T > 0$ there is a massive singularity at the center ($r = 0$). But the center does not remain at $R = 0$. The singularity is at $R = y_{ms} T$.

Another family of solutions, which we call "asymptotically Friedmann solutions" exists. In these solutions the whole $T = 0$ spacelike surface is singular. This singularity resembles the collapse to $r = 0$ of a closed Friedmann solution. We will not consider these solutions in this paper.

F. Exact solutions

We consider now a few exact solutions to the self-similar equations.

(1) *Dust.* Our perfect fluid becomes dust when $k=0$. The self-similar dust solution is a special case of the Tolman-Bondi solution. We will discuss this solution in Sec. VIII.

(2) *A static singular solution.* In this solution $u^r=0$. It follows from Eq. (2.9c) that λ is a constant ($\lambda=\lambda_0$), and it follows from Eq. (2.9a) that D is also a constant, with

$$D=\tfrac{1}{2}(1-e^{-\lambda_0})\equiv D_s \ , \tag{2.31}$$

$$\mathcal{M}=\mathcal{M}_0=1-e^{-\lambda_0}=2D_s \ . \tag{2.32}$$

The only metric function that depends on x is v:

$$e^{v}=x^{2\alpha} \ , \tag{2.33a}$$

with

$$\alpha=(k+1)D_s e^{\lambda_0}=\frac{(k+1)D_s}{1-2D_s} \tag{2.33b}$$

(we have chosen here an arbitrary integration constant). For a given k there is only one possible D_s value. This cannot be observed in Eqs. (2.9a)–(2.9d) since Eq. (2.9d) becomes trivial when $u^r=0$. We use, instead, the self-similar radial Euler equation (with $u^r=0$)

$$xv'=\frac{4k}{k+1} \tag{2.34}$$

to obtain [using also Eqs. (2.33a) and (2.33b)]

$$D_s=\frac{2k}{(k+1)^2+4k} \ . \tag{2.35}$$

The static solution [Eqs. (2.31), (2.32), (2.33a), (2.33b), and (2.35)] is of the same form for both the SSS and the SSC coordinates.

In this form of the solution it seems to be dependent. To discover the static nature of the solution we transform to $\hat{t}=t^{1-\alpha}$, and we find that

$$e^{\hat{v}}=(1-\alpha)^{-2}r^{2\alpha}, \quad u^{\hat{t}}=(1-\alpha)r^{-\alpha} \ . \tag{2.36}$$

It is clear that the static solution does not have a regular center. Therefore, it does not belong to the general group of solutions that we are interested in. However, this solution is a limit of a series of solutions with a regular center. We will discuss this in Sec. IV B.

(3) *The Friedmann solution.* The spatially flat cosmological Friedmann solution is also a self-similar solution. In this solution all the space becomes singular at $T=0$. It is a typical member of what we call an "asymptotically Friedmann solution." In SSC coordinates it looks like

$$e^{\Psi}=1, \quad e^{\Lambda}=\left[1-\frac{2}{3(k+1)}\right]^2|y|^{-4/(3k+3)} \ , \tag{2.37}$$

$$\tilde{D}=\frac{2}{3(k+1)^2}, \quad \tilde{r}=-|y|^{(3k+1)/(3k+3)} \ .$$

III. NEWTONIAN SELF-SIMILAR SOLUTIONS

A. An overview

We review in this section the Newtonian isothermal self-similar collapse model, which is the Newtonian analogue of the relativistic solutions that we are considering. This model was proposed by several authors[23–25] as an astrophysical model for collapse of interstellar clouds and formation of protostars. Here we are interested in it because it contains many features of the relativistic solution within a much simpler formalism, and without the relativistic coordinate singularities. We show latter that in the limit ($k\to 0, D_0=\lim_{x\to 0^-} Dx^{-2}\to$const) the relativistic solutions are approximately Newtonian: $\lambda \ll 1$, $u^r \ll 1$. Hence, we can predict many features of the relativistic solutions from consideration of their Newtonian analogue.

The Newtonian spherical motion of self-gravitating perfect fluid is described by three partial differential equations for the mass $m(r,t)$, the density $\rho(r,t)$, and the radial velocity $v(r,t)$. The Newtonian equations can be obtained directly or as a limit of Einstein's equations with $\lambda \ll 1$, $v \ll 1$, $|u^r| \ll 1$. In this limit u^r is identified with v.

Self-similarity is obtained from the condition

$$\begin{aligned} &v(r,t)=v(x) \ , \\ &\mathcal{M}(x)=\frac{m(r,t)}{r} \ , \\ &D(x)=4\pi r^2\rho(r,t) \ , \end{aligned} \tag{3.1}$$

where $x\equiv r/t$. The self-similar equations are ordinary differential equations:

$$(v-x)D'+Dv'=0 \ , \tag{3.2a}$$

$$(v-x)v'+\frac{kD'}{D}+\frac{\mathcal{M}-2k}{x}=0 \ , \tag{3.2b}$$

$$\mathcal{M}+x\mathcal{M}'=D \ , \tag{3.2c}$$

where a prime denotes, here, a derivative with respect to x. In self-similarity mass conservation leads to

$$\mathcal{M}=D\left[1-\frac{v}{x}\right] \ . \tag{3.3}$$

Hence there are only two independent variables D and v. We will consider solutions of Eqs. (3.2a)–(3.2c) with a regular center ($x=0^-$) for $t<0$. Regularity at $x=0^-$ requires $v(x=0^-)=0$. The regular solutions are fixed, therefore, by one parameter: D_0.

Newtonian solutions with different k and the same D_0 are related by a rescaling transformation. To see this consider the rescaled variables:

$$\begin{aligned} &\bar{x}=x/\sqrt{k} \ , \\ &\bar{v}=v/\sqrt{k}, \quad \bar{D}=D/k \ , \\ &\bar{\mathcal{M}}=\mathcal{M}/k \ . \end{aligned} \tag{3.4}$$

With these variables k disappears from the rescaled equations

$$(\bar{v}-\bar{x})\bar{D}'+\bar{D}\,\bar{v}'=0\ , \tag{3.5}$$

$$(\bar{v}-\bar{x})\bar{v}'+\frac{\bar{D}'}{\bar{D}}+\frac{\bar{\mathcal{M}}-2}{\bar{x}}=0\ , \tag{3.6}$$

$$\bar{\mathcal{M}}=\bar{D}\left[1-\frac{\bar{v}}{\bar{x}}\right]\ , \tag{3.7}$$

where a prime denotes, for a rescaled variable, a derivative with respect to $\bar{x}$. A solution of (3.5), (3.6), and (3.7) (with a regular center), a "general solution," is characterized by D_0. It represents a one-parameter family of physically different solutions (with different k values). There is no such relation between different self-similar relativistic solutions.

Just as in the relativistic case the density diverges at the center like $|t|^{-2}$ and the center becomes singular at $t=0$. We will focus our discussion on solutions in which at $t>0$ fluid shells collapse into the central singularity. The mass of this singularity grows linearly with t. These solutions are the Newtonian analogues of the relativistic "black-hole solutions."

Figures 1(a) and 1(b) describe a typical solution of this type. Figure 1(a) describes the precollapse part ($t<0$) while Fig. 1(b) describes the postcollapse part. One can see in Fig. 1(b) the divergence of $\bar{\mathcal{M}}$, $\bar{v}$, and $4\pi\rho t=\bar{D}\,\bar{x}^{-2}$ at $x=0^{+}$. Figure 2 describes the same Newtonian solution as function of $1/\bar{x}$. In this representation the continuous transition of the solution from $t<0$ to $t>0$ is manifest. $\bar{\mathcal{M}}$ and $|\bar{v}|$ increase monotonically. The density increases initially due to the collapse. Once the massive singularity is formed at the center, its strong gravitational field attracts the fluid in its neighborhood and the density for a given r decreases. This behavior is manifest in the graph of $\bar{D}(1/\bar{x})$.

The Newtonian gravitational potential, ψ, is given by

$$\frac{\partial\psi}{\partial r}=\frac{m}{r^2}=\frac{\mathcal{M}}{r}\ , \tag{3.8}$$

which leads to

$$\frac{\partial\psi}{\partial x}=\frac{\mathcal{M}}{x}\ . \tag{3.8a}$$

We choose $\psi(x=0^{-})=0$ so that

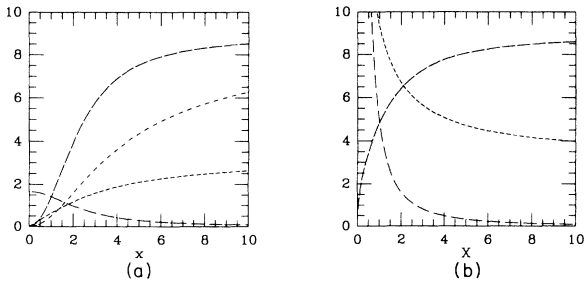

FIG. 1. The Newtonian Penston-Larson solution. The short dashed line is $-\bar{v}$, the long dashed line is $\bar{D}$, the short dashed dotted line is $\bar{\mathcal{M}}$, and the long dashed dotted line is $4\pi\rho t^2$. (a) describes the solution at $t<0$ and (b) for $t>0$.

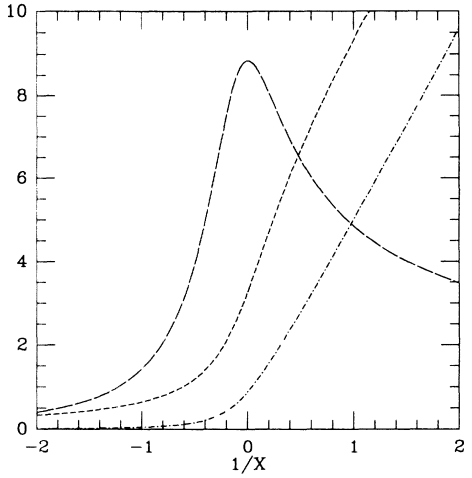

FIG. 2. The Penston-Larson solution as a function of $1/\bar{x}$. The short dashed line is $-\bar{v}$, the long dashed line is $\bar{D}$, and the short dashed-dotted line is $\bar{\mathcal{M}}/10$.

$$\psi=\psi(x)=\int_0^x\frac{\mathcal{M}(x)}{x}dx\ . \tag{3.9a}$$

We define a rescaled gravitational potential $\bar{\psi}\equiv\psi/k$, and we obtain

$$\bar{\psi}(\bar{x})=\int_0^{\bar{x}}\frac{\bar{\mathcal{M}}(\bar{x})}{\bar{x}}d\bar{x}\ . \tag{3.9b}$$

The Newtonian limit ($k\to 0$, $e^{\nu}\approx 1$) of Eq. (2.9b') yields $\nu'=2\mathcal{M}/x=2\psi'$. Since $\nu(0)=\psi(0)=0$, we find that in this limit, $\nu=2\psi$.

At $t=0$ all these solutions have a particularly simple form,

$$\begin{aligned} v(r,0)&=\sqrt{k}\,\bar{v}_\infty\ ,\\ \rho(r,0)&=\frac{k\bar{D}_\infty}{4\pi r^2}\ ,\\ m(r,0)&=k\bar{\mathcal{M}}_\infty r=k\bar{D}_\infty r\ , \end{aligned} \tag{3.10}$$

which resembles the form of a static Newtonian solution (this would have been the case if $v_\infty=0$). An asymptotic expansion to first order in $1/\bar{x}$ near $1/\bar{x}=0$ depends on two parameters, $\bar{D}_\infty$ and $\bar{v}_\infty$:

$$\begin{aligned} \bar{v}&=\bar{v}_\infty+\frac{\bar{v}_{1\infty}}{\bar{x}}+O(\bar{x}^{-2})\ ,\\ \bar{D}&=\bar{D}_\infty+O(\bar{x}^{-2})\ ,\\ \bar{\mathcal{M}}&=\bar{D}_\infty-\bar{D}_\infty\bar{v}_{1\infty}\bar{x}^{-1}+O(\bar{x}^{-2})\ , \end{aligned} \tag{3.11}$$

and

$$\bar{\psi}=\bar{D}_\infty\ln\bar{x}+\bar{\psi}_\infty-\bar{D}_\infty\bar{v}_\infty x^{-1}+O(X^{-2}) \tag{3.12}$$

(with $v_{1\infty}=2\bar{D}_\infty$). ψ_∞ is, clearly, just a constant of integration. The divergence of ψ at $t=0$ suggests that ν will diverge at $t=0$ in the relativistic solution and that the line $t=0$ will be singular. This is indeed the case but this singularity is just a coordinate singularity of the SSS coordinates.

All the solutions of Eqs. (3.5) and (3.6) pass through a "sonic point" x_{sp}, defined by $\bar{v}-\bar{x}=\pm 1$. The system of equations is degenerate at this point. Some solutions are not extendible beyond x_{sp}. Other solutions can be extended in a smooth but not analytic manner. (All the derivatives of $\bar{v}$ and $\bar{D}$ higher than some order diverge at $\bar{x}_{sp}$.) There is only a discrete set of solutions that pass through the sonic point analytically. Ori and Piran[19] have shown that all the nonanalytic solutions are unstable to a development of a kink (a discontinuity in the velocity and density gradients) at x_{sp} (Ref. 31). Among the discrete set of analytic solutions at x_{sp} there are only two for which $\bar{v}\leq 0$ everywhere. One is the homogeneous solution (the Newtonian analogue of the time-reversal Friedmann solution). The homogeneous solution is also unstable to a development of a kink at x_{sp}. The other is the "black-hole-type" Penston-Larson solution which was described in Figs. 1 and 2.

B. The relations between Newtonian and relativistic solutions

Generally when a Newtonian solution satisfies

$$|\mathcal{M}|\ll 1,\quad |\psi|\ll 1,\quad |v|\ll 1\ , \tag{3.13}$$

one can expect that it will be a good approximation to corresponding relativistic solution. The approximation improves when the last inequality becomes stronger.

For any $x\neq 0$ and $x\neq\infty$, $\lim_{k\to 0}\bar{x}(x)=\pm\infty$. Hence, $\lim_{k\to 0}v(x)=\lim_{k\to 0}(\sqrt{k}\ \bar{v}_{\infty})$, $\lim_{k\to 0}D(x)=\lim_{k\to 0}(k\bar{D}_{\infty})$. It follows that when $\bar{D}_{\infty}$ and $\bar{v}_{\infty}$ are finite we can choose small enough k such that $\psi(x)$, $v(x)$, $\mathcal{M}(x)$, and $D(x)$ will be arbitrarily small for any given $x\neq 0^{+}$. The condition that $\bar{D}_{\infty}$ and $\bar{v}_{\infty}$ are finite holds for "black-hole-type" solutions but is not valid for "asymptotically Friedmann" solutions. For "black-hole-type" solutions we find that, for a fixed x,

$$\lim_{k\to 0}\mathcal{M}=\lim_{k\to 0}v=\lim_{k\to 0}\psi=0\ . \tag{3.14}$$

Thus, in the limit $k\to 0$ a given relativistic solutions is well approximated by some Newtonian solution (see Fig. 18). Similarly, in this limit, the relativistic solutions are related by a rescaling transformation equivalent to Eq. (3.4).

When we take the limit [Eq. (3.14)] we hold $\bar{D}$ and $\bar{v}$ constant. When we perform the corresponding limit for the relativistic solutions we let D/k and $u^{r}/\sqrt{k}$ approach a finite function (of $\bar{x}$) (in particular D_0 approaches also a constant value). One can use another limiting process, in which D and u^{r} approach a constant function (of x). In this limit we obtain the relativistic dust solutions (see Sec. VIII).

Every Newtonian solution (of a "black-hole type") contains, however, a strong field region near the massive singularity at $x=0^{+}$, where ψ, v, D, and $\mathcal{M}$ diverge [see Fig. 1(b)]. Near $t=0$ there is a region where ψ diverges but v, D, and m are finite and small. This reflects the divergence of v and the breakdown of the SSS coordinates at $t=0$. As k decreases both regions become narrower (both in terms of x and of $\bar{x}$). In particular the line $x=1$ ($r=t$) is located in a weak-field region for small enough k. In the limit $k\to 0$ the weak-field region becomes flat and $r=t$ is null. In Sec. V we use this limiting procedure to demonstrate the appearance of naked singularities in relativistic solutions with small enough k values.

IV. A GENERAL DESCRIPTION OF RELATIVISTIC SOLUTIONS

A. The numerical solution

To obtain a general relativistic solution we solve numerically Eqs. (2.9a)–(2.9d) (for SSS) and (2.20a)–(2.20d) (for SSC). These are ordinary nonlinear differential equations that we solve using standard numerical techniques. To check the accuracy of our solutions we have performed the following tests: (1) comparison of the solution with different grid sizes; (2) comparison of the solutions in the two different coordinate systems; (3) comparison with analytic solutions like Friedmann or dust; (4) comparison with the Newtonian limit (when it is valid); (5) comparison with the analytic asymptotic expansions.

The results that we present here are significant to at least four digits. There is no numerical problem in improving this accuracy. However, none of the properties of the solution that we describe depend critically on the accuracy of the solution.

The set of Eqs. (2.9a)–(2.9d) and (2.20a)–(2.20d) contain some singular points (e.g., the sonic point, the regular center, the massive singularity, and coordinate singularities) which we discuss. In these points we always expand the solution analytically [see, e.g., Eqs. (2.15a)–(2.15e)]. We use these expansions both to overcome the numerical problems at these points and to study analytically the behavior of the solutions there. In fact the numerical solution is needed mostly to bridge between these asymptotic expansions.

B. The sonic point and the space of relativistic solutions

We have seen earlier that for a given k a self-similar solution is characterized, locally, by two parameters [D_0 and $u^{r}(0)$]. In the regular solutions (before $T=0$) that we consider, the velocity u^{r} vanishes at the center, and such solutions are characterized near the origin by D_0. However, D_0 characterizes the solution only up to the "sonic point" which we denote $x=x_{sp}$ ($y=y_{sp}$). At this point the fluid moves at the speed of sound relative to the self-similarity line $x=x_{sp}$. The self-similar equations [Eqs. (2.9a)–(2.9d), (2.20a)–(2.20d)] are degenerate at $x=x_{sp}$. The behavior of the solutions at the sonic point resembles the behavior of the Newtonian solutions.[26–28] We discuss the behavior of the solutions at the sonic point in Sec. VII. In this section we consider briefly the implication of the existence of the sonic point on the space of solutions.

In some solutions D' and u'' diverge at the sonic point and the solution cannot be extended beyond it. We will consider, in the sequel, only solutions for which all (first-order) derivatives are finite at x_s and the solution can be continued beyond it (without a shock wave) in a self-

similar manner. This requirement forms a "band structure" in the space of solutions. The D_0 line is divided into an infinite set of "permitted" segments (for which the solutions can be continued) and "forbidden" segments (for which the solutions necessarily terminate at the sonic point). In every "permitted" band, only few solutions are analytic at x_{sp}. All the other solutions are smooth, but not analytic there.

The sonic point is, generally, a branching point in the solution. Therefore, an additional parameter is required to specify the solution beyond x_{sp} and the space of solutions is a two parameter set for $|x|>|x_{sp}|$. On the other hand, if one focuses on solutions which are analytic at x_{sp}, the space of solutions is reduced to a discrete set (there is a discrete set of D_0 values for which x_{sp} is approached analytically, and for every such solution there is only one analytic continuation beyond x_{sp}). (See Sec. VII.)

A similar structure of infinite bands exist also in the Newtonian model. Whitworth and Summers[28] have shown that every band has its own typical velocity profile. In the first band $u^r<0$, corresponding to a "pure collapse" solution that collapses everywhere. In the second band $u^r<0$ near the origin and it changes sign at least once but not more than twice. This solution collapses at the origin but has an expanding region (which may or may not reach infinity). The nth band has a collapsing region near the origin and $n-1$ expanding regions separated by collapsing regions. The limits between the collapsing and expanding regions are self-similarity lines which move relative to the matter and reach the origin at $t=0$.

After checking (numerically) a range of the parameter space ($0<k\leq\frac{1}{3}$) we have found that a similar behavior appears in the relativistic model, at least for the first two bands. This typical behavior is shown in Figs. 3(a) and 3(b).

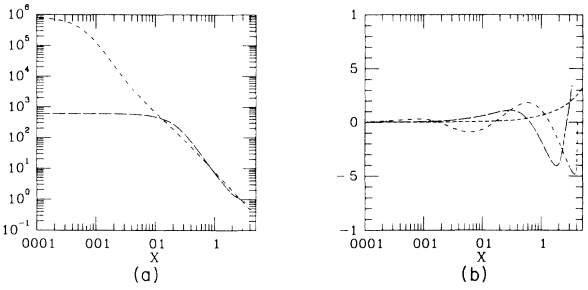

FIG. 3. Three self-similar solutions for $k=0.05$. (a) displays $4\pi\rho t^2$ and (b) displays $-10^{n-1}u^r$. The short dashed line denotes the solution with $D_0=0.85$, the long dashed line—$D_0=600$, and the short dashed-dotted line—$D_0=800\,000$. The variance in the density profile of the $D_0=0.85$ solution (from 0.85 at $x=0$ to 0.79 at x_{sp}) is not apparent because of the large logarithmic scale used in (a). One can see that when n increases (here from 1 to 3) the density profile approaches a straight line (in log-log coordinates). This straight line corresponds to $D\propto x^{-2}$, which is the density profile of the static solution (see Sec. II E). In (b) the extension factor of 10^{n-1} expresses the fact that as $n\rightarrow\infty$, $u^r\rightarrow 0$.

When we increase n the number of nodes in the velocity profile increases and the absolute value of the velocity decreases. Thus, at the limit $n\rightarrow\infty$, $u^r\rightarrow 0$, and the solution approaches the static solution (see Sec. II F). This behavior, which was discussed in Ref. 11, is demonstrated in Figs. 3(a) and 3(b) (in which the vertical scale of the nth order solution is extended by a factor of 10^{n-1}).

There are only two analytic (at x_p) "pure collapse" families of solutions: the Friedmann solutions [with $D_0=2/3(k+1)^2$] and the general-relativistic generalization of the Newtonian Penston-Larson (GRPL) solutions (which exist for $0<k<k_p\approx 0.036\pm 0.002$).

C. Classification of the relativistic solutions

We divide the solutions to three different classes according to the behavior at $T\geq 0$. For this purpose it is useful to define the quantities

$$D=D_T,\quad \mathcal{M}=\mathcal{M}_T,\quad u^r=u^r_T\ , \tag{4.1}$$

on the self-similar line $T=0$.

(1) *Black-hole solutions.* In these solutions a massive singularity forms at the center at $T=0$. The mass of the singularity grows linearly with T.

(2) *Asymptotically Friedmann solutions.* In these solutions u^r_T, D_T, and $\mathcal{M}_T$ diverge at $T=0$. The situation resembles the "big crunch" when all the universe collapses to one point.

(3) *Repulsive solutions.* In repulsive solutions the central singularity, that forms at $T=0$ disappears instantaneously and the fluid expands regularly afterward. A particular case of these solutions is the time symmetric case in which the expansion is a time reversal of the collapse. In the time-symmetric solutions $u^r_T=0$.

An interesting subclass of these solutions are the *explosion solutions*. These are solutions with a large positive u^r_T. They contain a central collapsing core surrounded by an expanding envelope before $T=0$. The density of the central core grows (like T^{-2}) but its mass decreases (like $|T|$). At $T=0$ all the fluid shells move outward with $u^r_T>0$. For $T>0$ these shells are accelerated outward with velocities approaching the speed of light. A vacuum region forms at the center, whose boundary is the light cone emerging from the singularity at (0,0) (see Fig. 4). These solutions do not have a Newtonian analogue. We will discuss these solutions in a separate publication.

In the "black-hole" and repulsive solutions U^r_T, D_T, and $\mathcal{M}_T$ are finite. When $u^r_T\ll 0$ we have a "black-hole" solution, when $u^r_T\gg 0$ we have an exploding solution. When $|u^r_T|$ is relatively small the solution has a second sonic point at $T>0$. Some solutions terminate at this sonic point. Those that can be continued are either a "black-hole"-type or repulsive solutions.

D. "Black-hole"-type solutions

From now on we will discuss only "black-hole"-type solutions. The asymptotically Friedmann solutions have been considered by Carr and Yahil[14] (asymptotically Friedmann solutions without a regular center have been

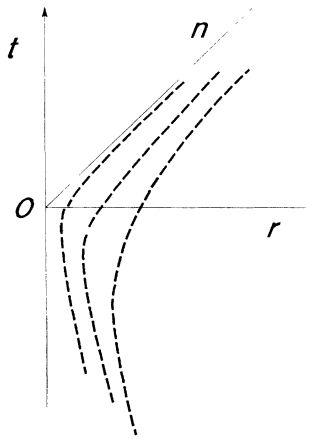

FIG. 4. A schematic space-time diagram for an "explosion solution" in $r-t$ coordinates. Each fluid shell initially collapses and then (when it intersects the dotted line) it expands approaching asymptotically the speed of light. The line n denotes the light cone of the (0,0) density singularity. n is also the boundary between the fluid exterior and the expanding vacuum interior.

considered by Carr and Hawking[12] and Bicknell and Henriksen[13]). We will discuss the explosive solutions elsewhere.

Figure 5 is a schematic space-time diagram of a "black-hole" solution in SSC coordinates. Figures 6 and 7 describe a $k=0.01$ GRPL solution in SSC coordinates [Figs. 6(a) and 6(b) for $T<0$ and Figs. 7(a) and 7(b) for $T>0$]. Figures 7(a) and 7(b) display a singularity at $y=y_{\rm ms}$ where D, u^r, and M diverge and $\bar{r}=0$. The matter shells collapse into the central singularity along $y=y_{\rm ms}$ (see Fig. 5). The asymptotic behavior near y_s is given by

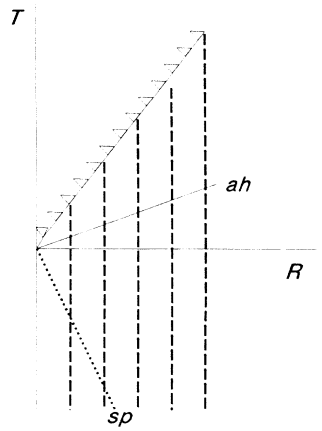

FIG. 5. A schematic space-time diagram of a "black-hole-type" solution in comoving coordinates. ah is the apparent horizon and sp is the sonic point. The dashed lines denote the world lines of the fluid shells.

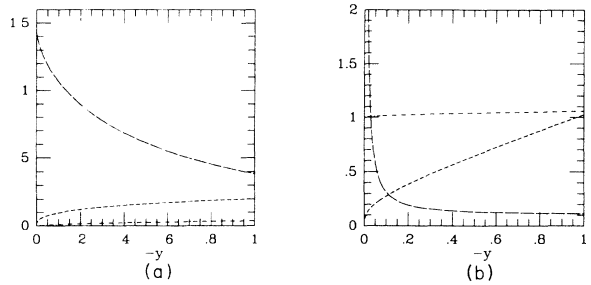

FIG. 6. A typical "black-hole" solution—the $k=0.01$ GRPL solution in comoving coordinates at $T<0$. (a) The short dashed line is $-u^r$, the long dashed line is $4\pi\rho t^2$, and the short dashed-dotted line is m/r. (b) The short dashed line is $\bar{r}$, the long dashed line is $-g_{RR}$, and the short dashed-dotted line is g_{TT}.

$$D\approx D_{\rm ms}\delta y^{1/3-k},\quad \bar{r}\approx\bar{r}_{\rm ms}\delta y^{2/3},$$
$$\mathcal{M}\approx\mathcal{M}_{\rm ms}\delta y^{-2/3},\quad u^r\approx u_{\rm ms}\delta y^{-1/3}, \tag{4.2}$$
$$e^{\psi}\propto\delta y^{2k},\quad e^{\Lambda}\propto\delta y^{-2/3},$$

where $\delta y\equiv(y-y_{\rm ms})^{1/(1-k)}$. One can show that this asymptotic behavior is characterized by two free parameters. It follows directly from the form of the metric functions that the singularity at $y_{\rm ms}$ is spacelike. The divergence of $\mathcal{M}$ at the singularity is related to the fact that the singularity is massive. The mass of the singularity grows linearly with T:

$$\frac{m_{\rm singularity}}{T}=\lim_{y\to y_{\rm ms}}\mathcal{M}\bar{r}=\mathcal{M}_{\rm ms}r_{\rm ms}=\text{const}\ . \tag{4.3}$$

The divergence of $\mathcal{M}$ also indicates that there are trapped surfaces near the massive singularity. Hence there is a black hole in these solutions.[32]

We will return to the description of the asymptotic behavior near the massive singularity at Sec. VI where we will be using SSS coordinates.

The SSC coordinates become singular at two other self-similar lines.

(1) $T=0$ where g_{TT} diverges:[33]

$$g_{TT}\propto y^{4k/(k+1)}\ . \tag{4.4}$$

(2) $R=0$ (the regular center) where g_{RR} diverges:

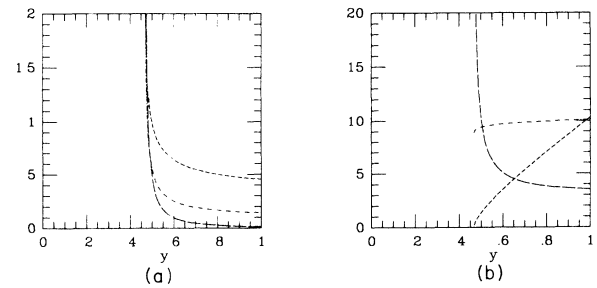

FIG. 7. The $T>0$ part of the $k=0.01$ GRPL solution. The notations are the same as in Fig. 6 (correspondingly). The $y_{\rm ms}$ singularity is located at $y\approx0.47$.

$$g_{RR} \propto y^{-4/[3(k+1)]} . \quad (4.5)$$

These are only coordinate singularities which can be bypassed by using SSS coordinates or other comoving coordinates which are not SSC.

A different set of coordinates that are particularly useful for a global description of the space-time are (τ,r) coordinates where r is an area coordinate and τ is the proper time measured by an observer comoving with the matter. To define τ uniquely we fix $\tau=0$ along $T=0$. One can easily verify that all the self-similarity lines are of the form $r/\tau=$const. Figure 8 describes the schematic form of the "black-hole" solutions in these coordinates. The massive singularity is located at $r=0^+$ and it grows linearly with τ.

V. NULL GEODESICS

A. General structure

The radial null geodesic (RNG) equation in a spherically symmetric space-time with a diagonal metric is

$$\frac{dR}{dT}=\pm\left[\frac{-g_{TT}}{g_{RR}}\right]^{1/2} , \quad (5.1)$$

where the plus corresponds to an outgoing geodesic and the minus to an ingoing one. In a self-similar space-time Eq. (5.1) is of the form

$$\frac{dR}{dT}=f(R/T) . \quad (5.2)$$

An important group of solutions of Eq. (5.2) are solutions of the form $R=y_0T$, where y_0 is a constant. We call these solutions "simple RNG's." The other geodesics will be called "curved RNG." The negative (positive) solutions of the algebraic equation

$$F(y)\equiv-\frac{y^2g_{RR}(y)}{g_{TT}(y)}=1 , \quad (5.3)$$

describe ingoing (outgoing) simple RNG's that reach (leave) the singularity at (0,0). We denote by $y_1^+,\ldots,y_n^+$ all the positive solutions of Eq. (5.3) with $y_1^+,>y_2^+>\cdots>y_n^+>y_{\rm ms}$. y^- is the solution describing a simple ingoing geodesic.

If $R(T)$ is a solution of Eq. (5.2) then, for every $a>0$,

$$R_a(T)\equiv aR(T/a) , \quad (5.4)$$

is also a solution. A simple RNG is invariant under the transformation (5.4), but the curved RNG's are not. Hence, using Eq. (5.4) we can generate a one-parameter family of curved RNG's from any given curved RNG. Since radial null geodesics (RNG) are a one-parameter family of solutions all the RNG's are divided into a small number of equivalent classes. In every such equivalent class all the RNG's are related by the transformation (5.4).

The simple RNG's play a central role in the causal structure. To show that we first write Eq. (5.1) as

$$\frac{dy}{dl}=\frac{dR}{dT}-\frac{R}{T}=\pm\left[-\frac{g_{TT}}{g_{RR}}\right]^{1/2}-y=\pm\frac{|y|}{F}-y \equiv g^{\pm}(y) , \quad (5.5)$$

where $l\equiv\ln T$ and the plus-minus sign correspond to outgoing and ingoing geodesics. The simple RNG's satisfy $g^{\pm}(y)=0$. Consider now, for example, the RNG's in the range $y_2^+<y<y_1^+$. Outgoing RNG's cannot cross each other (apart from in a singular point). Hence these geodesics do not cross y_1^+ or y_2^+. g^+ has a constant sign in this range since it does not vanish there. According to Eq. (5.5) an RNG, $y(l)$, in this range will be a monotonous function. Defining $y_{\pm\infty}\equiv\lim_{l\to\pm\infty}y(l)$. We obtain $y_2^+\le y_{\pm\infty}\le y_1^+$. g^+ must vanish for both $y_{+\infty}$ and $y_{-\infty}$; hence, they must coincide with y_{1+} and y_{2+}. Suppose that $g^+>0$ then $y_{+\infty}=y_1^+$ and $y_{-\infty}=y_2^+$. Such RNG spans the whole range (y_2^+,y_1^+). It is tangent to y_2^+ at (0,0) (which corresponds to $l=-\infty$) and it is tangent to y_1^+ at $T\to\infty$. The role of y_1^+ and y_2^+ is reversed if $g^+<0$. In every point (R,T) in the range $y_2^+<y<y_1^+$ one can find an outgoing RNG which is equivalent to $y(l)$ [by means of Eq. (5.4)]. This new geodesic is obtained from the original one by the simple transformation $l\to l+l_0$ (with some constant l_0). Since only one outgoing RNG passes through any point (R,T), all the outgoing RNG's in the range $y_2^+<y<y_1^+$ belong to the same equivalence class. Figure 9 describes, schematically, this structure. Similar behavior appears between any pair of

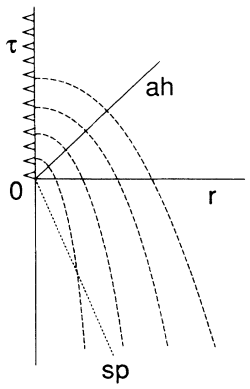

FIG. 8. A schematic space-time diagram of a "black-hole-type" solution in (r,τ) coordinates. The notation is the same as in Fig. 5.

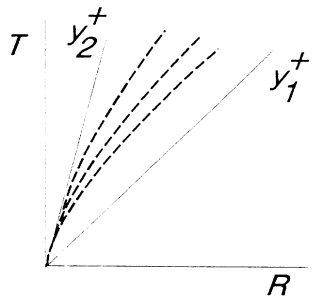

FIG. 9. A schematic description of outgoing RNG's (dashed lines) between two simple outgoing RNG's, y_1^+ and y_2^+.

simple RNG's.

The situation is different in the two extreme ranges $y_{ms} < y < y_n^+$ and $1/y < 1/y_1^+$. The curved RNG's do not span the whole range $-\infty < l < \infty$, but terminate at the regular center (or y_{ms}) in a finite l value, i.e., a nonzero finite T value (see Fig. 10). For y_{ms} this is evident from Eq. (4.2), which reads $g^{\pm}(y_{ms}) = -y_{ms} > 0$. For the regular center, this behavior is clear when one uses SSS coordinates (see Sec. V F) in which $\bar{g}^{\pm}(0^-) = \pm 1$. Consequently, if $n = 0$ (i.e., there are no simple outgoing RNG's), all the outgoing RNG's leave $R = 0^-$ in finite $T < 0$ values and reach y_{ms} in finite $T > 0$ values.

The divergence of l on the line $T = 0$ does not indicate any special feature of this line, and the RNG's cross it (in finite R values) from the $y < 0$ to $y > 0$ without any problems (this is also evident when one uses SSS coordinates, in which the line $T = 0$ has no special rule).

This analysis can be repeated for ingoing RNG's. We conclude therefore that if there are n simple outgoing (ingoing) RNG's, they divide the curved outgoing (ingoing) RNG's into $n+1$ equivalence classes, and correspondingly divide the $R - T$ plan into $n+1$ ranges, with a one-to-one correspondence.

In the next two sections we apply that analysis to recover the structure of ingoing and outgoing RNG's.

B. Ingoing geodesics

Figure 11 describes F for $y < 0$. One can verify from Eqs. (5.3), (4.4), and (4.5) that $\lim_{y \to \infty} F(y) = \infty$ and $F(0^-) = 0$. Hence, there exists at least one point y^- for which $F(y^-) = 1$. In all the "black-hole-type" solutions that we have studied there is only one such point (in other types of solutions there might be more then one such point) and there is only one ingoing simple RNG. Figure 12 describes schematically the ingoing geodesics in a "black-hole-type" solution.

C. Outgoing geodesics

We divide the "black-hole-type" solutions to solutions containing a naked singularity and solutions that do not contain one. Figure 13 describes the functions F and g^+ in the range $T > 0$, for a few solutions. $\lim F = +\infty$ for both $y \to y_{ms}$ [Eq. (4.2)] and $y \to \infty$ [Eq. (4.4)]. F has a minimal value F_{min} between this two values. When

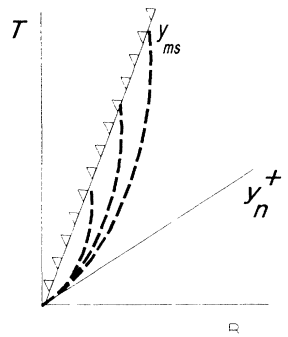

FIG. 10. A schematic description of outgoing RNG's between y_{ms} and the last simple outgoing RNG y_n^+.

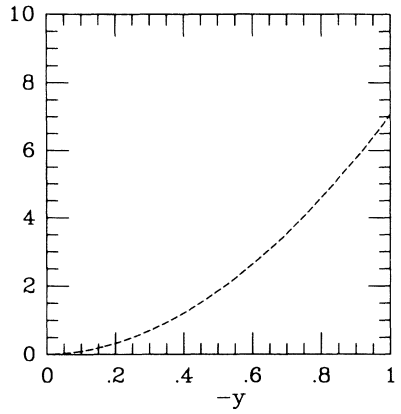

FIG. 11. F as a function of $-y$ (for $T < 0$) for the $k = 0.01$ GRPL solution.

$F_{min} > 1$ there are no simple outgoing RNG and the singularity at (0,0) is not naked (see Fig. 14). In these solutions all the outgoing geodesics terminate at the massive singularity. When $F_{min} < 1$ there are two values y_1^+ and y_2^+ for which $F = 1$. In this case the singularity at (0,0) is naked. The outgoing simple RNG's at y_1^+ and y_2^+ and all the curved RNG's between them reach infinity (see Fig. 15). y_1^+ is a Cauchy horizon and y_2^+ is the event horizon. All the outgoing geodesics that leave (0,0) in the range $y_{ms} < y < y_2^+$ are initially tangent to y_2^+. In these geodesics r increases initially (with T) until the apparent horizon y_{ah} is reached. r decreases later and the massive singularity at y_{ms} is reached within a finite T value.

D. Naked singularity solutions

A numerical study reveals that for every k in the range that we have studied ($0 \le k \le 0.4$) there are solutions with naked singularities. The existence of these solutions is evident from the following arguments.

In Sec. III we have discussed the Newtonian limit at $k \to 0$. We take a series of "black-hole-type" solutions with k values approaching zero, such that both D/k and $u^r/\sqrt{k}$ approach limiting functions of $\bar{x} = x/\sqrt{k}$. These functions correspond to a Newtonian solution of Eqs. (3.5)–(3.7). Consider now the line $\bar{x} = 1$. On this line we have, for $k \to 0$, $\nu \approx \psi \approx k\bar{\psi}(\bar{x} = 1)$, and $\mathcal{M} \approx k\bar{\mathcal{M}}(\bar{x} = 1)$.

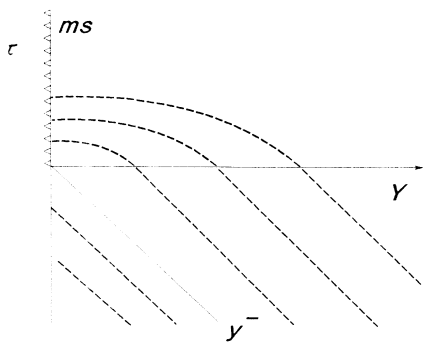

FIG. 12. A schematic description of incoming RNG's in a "black-hole-type" solution.

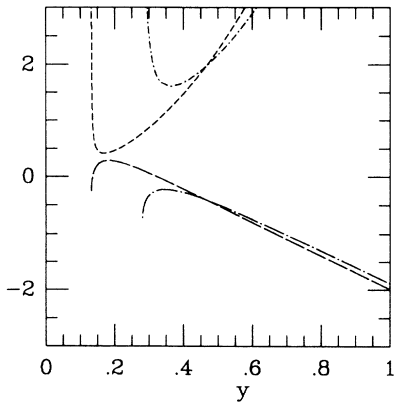

FIG. 13. F and g^+ at $T>0$ for two "black-hole-type" solutions. One (the dashed lines) is the $k=0.005$ GRPL solution, which contains a naked singularity. The other (the dashed-dotted lines) is the $k=0.015$ GRPL solution, in which there is no naked singularity. The short dashed and dashed-dotted lines denote F, and the long dashed and dashed-dotted lines denote g^+.

Hence $-g_{rr}x^2/g_{tt}\approx x^2=k$. Since $k<1$ this line is timelike and future directed. Therefore, for small enough k the singularity at (0,0) is naked.

In Sec. IV we have mentioned that the space of solution is divided into a set of bands. For a given k, we take a series of solutions with each member in a higher n band. This series will approach the static singular solution (provided that one chooses the appropriate continuation at x_{sp}). Since the latter is naked (with $F_{min}=0$) all the solutions in that series with sufficiently high n have $F_{min}<1$, and their singularity at (0,0) is naked.

According to these two arguments solutions with small k or with $n>1$ (i.e., solutions with oscillations in the velocity field) are expected to contain naked singularities. The numerical studies suggest that these are the only self-similar solutions with naked singularities. For example, all the GRPL solutions with $k<k_c\approx 1.0105$ are naked, but those with $k>k_c$ are not. It seems that all the "pure collapse" solutions with $k>k_c$ are not naked. On the other hand, in the second band there are naked singular solution for every k.

It is clear that the subset of naked singular solution is of nonzero measure in the three-dimensional space of self-similar spherical solutions.

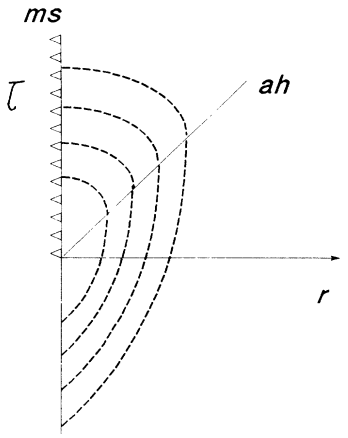

FIG. 14. A schematic description of outgoing RNG's (dashed lines) in r,τ coordinates for "black-hole-type" solutions without a naked singularity.

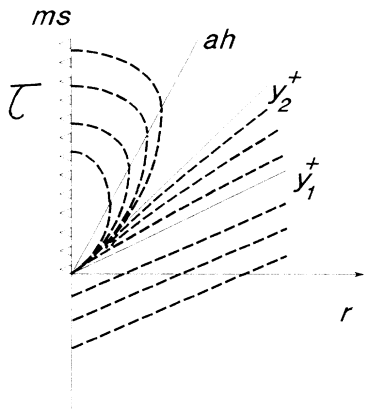

FIG. 15. A schematic description of outgoing RNG's (dashed lines) in r,τ coordinates for "black-hole-type" solutions with a naked singularity.

E. Penrose diagrams

Figures 16 and 17 describe the Penrose diagrams of both types of solutions. In the naked singularity solutions different RNG's emerge from the singularity at (0,0), hence the singularity at (0,0) is not a point but an ingoing null line. In solutions without a naked singularity all null or timelike curves terminate at the massive singularity. In consequence, there is no future null boundary in Fig. 17.

This causal structure corresponds to the structure of

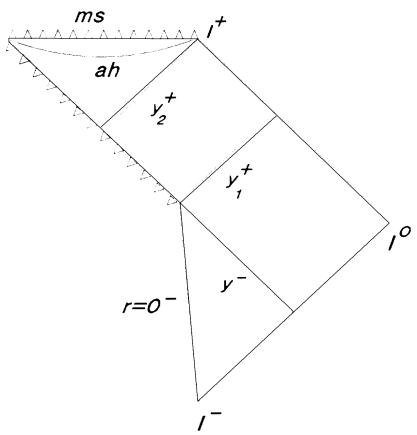

FIG. 16. Penrose diagram for "black-hole-type" solutions with a naked singularity.

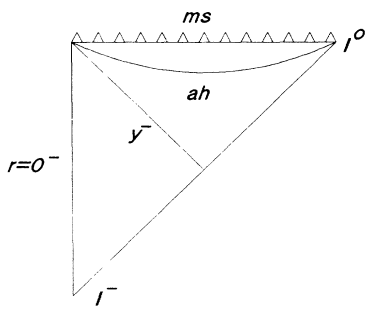

FIG. 17. Penrose diagram for "black-hole-type" solutions without a naked singularity.

complete self-similar solutions, which are not asymptotically flat. To obtain an asymptotically flat solution we introduce a cutoff (see Sec. VI) and match the solution to a non-self-similar region. If the cutoff is done far enough it does not change the nature of the overall causal structure of the solution with a naked singularity. For solutions without a naked singularity the cutoff changes the overall structure as a future null infinity and an event horizon appear.

F. RNG's in SSS coordinates

Some features of the solution are easier to grasp in SSS coordinates. The analysis of null geodesics in SSS coordinates is completely analogous to the one in SSC coordinates. The RNG equation in SSS coordinates is

$$\frac{dr}{dt}=\pm\left[-\frac{g_{tt}}{g_{rr}}\right]^{1/2} . \tag{5.6}$$

In terms of x and $\sigma\equiv\ln t$ Eq. (5.6) becomes

$$\frac{dx}{d\sigma}=\pm\left[-\frac{g_{tt}}{g_{rr}}\right]^{1/2}-x\equiv\bar{g}^{\pm}(x) . \tag{5.7}$$

The simple outgoing (ingoing) RNG's of the form $r=x_i^{\pm}t$ satisfy $\bar{g}^{+}(x_i^+)=0[\bar{g}^{-}(x^-)=0]$, where x^-,x_1^+,x_2^+, etc., correspond to y^-,y_1^+,y_2^+, etc., $x^-,x_1^+,x_2^+,\ldots$ are also the roots of the algebraic equation

$$\bar{F}(x)\equiv-\frac{x^2g_{rr}(x)}{g_{tt}}=1 . \tag{5.8}$$

$\bar{F}$ vanishes at $x=0^-$ [see Eq. (2.15)] and diverges at limits $x\to\infty$ ($t\to\infty$) and $x\to0^+$ [see Eqs. (6.11)]. There is a minimal value $\bar{F}_{\min}$. $\bar{F}$ has a naked singularity if $\bar{F}_{\min}<1$.

In all the naked singularity solutions we need four SSS coordinate patches to cover the whole space-time. x^- is located in the first patch $t<0$. x_1^+ and x_2^+ are at the second patch ($0<t$); hence, all the outgoing RNG's that reach infinity remain in the first two SSS patches. These are the two patches that admit a Newtonian weak field approximation. One can use the Newtonian approximation to study the simple RNG's x^- and x_1^+ (but not x_2^+). In this limit $e^{\nu},e^{\lambda}\to1$, and $\bar{F}\to x^2$. Hence, $\lim_{k\to0}x^-=-1$ and $\lim_{k\to0}x_1^+=+1$ (x_2^+ does not exist in this approximation it is located in the narrow strong field region near $x=0^+$). Figure 18 describes $\bar{F}$ and the Newtonian approximation to $\bar{F}$ for a few GRPL solutions.

G. The redshift

We turn now to the redshift

$$z=\frac{dt_0}{dt_s}\left[\frac{g_{tt}(r_0/t_0)}{g_{tt}(0^-)}\right]^{1/2} \tag{5.9}$$

along a geodesic $x(t)$ that emerges from a source at the center at t_s and reaches an observer at $r=r_0=$const at t_0. We calculate z at the limit $t_s\to0$ and we find the redshift along the geodesic x_1^+ that leave the singularity at (0,0) when it is naked (see Fig. 19).

We denote

$$\delta x(t)\equiv x(t)-x_1^+ . \tag{5.10}$$

$\lim_{t_s\to0}x(t)=x_1^+$; hence, $\lim_{t_s\to0}\delta x=0$. $\delta x(t)$ satisfies the same differential equation as $x(t)$, Eq. (5.7). It follows from the self-similar structure of the solution [or from a direct solution of Eq. (5.7)] that the dependence of δx of the parameter t_s is of the form

$$\delta x=\delta x(t/t_s) . \tag{5.11}$$

On the other hand we can, in the limit that we consider, expand $\bar{g}^{+}$ to first order in δx to obtain, from Eq. (5.7),

$$\frac{d\delta x}{d\sigma}\approx\left[\frac{d\bar{g}^{+}}{dx}\right]_{x=x_1^+}\delta x\equiv\bar{G}\delta x \tag{5.12}$$

and

$$\delta x\approx ae^{\bar{G}\sigma}=at^{\bar{G}} , \tag{5.13}$$

where a determines the geodesic and it is fixed by t_s. Comparison of Eqs. (5.11) and (5.13) yields

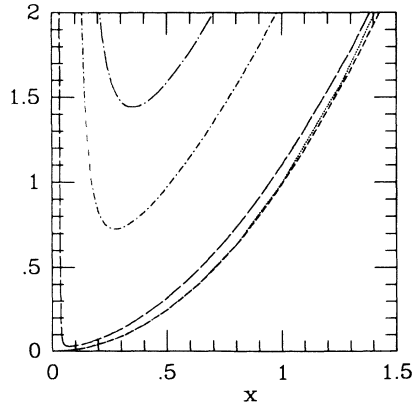

FIG. 18. $\bar{F}(x)$ for GRPL solutions. The short dashed line—for $k=0.001$, the long dashed line for $k=0.005$, the short dashed-dotted line for $k=0.01$, the long dashed-dotted line for $k=0.011$. The dotted line denotes the Newtonian limit $k\to0$, for which $\bar{f}(x)=x^2$. All these solutions contain a naked singularity except that with $k=0.011$.

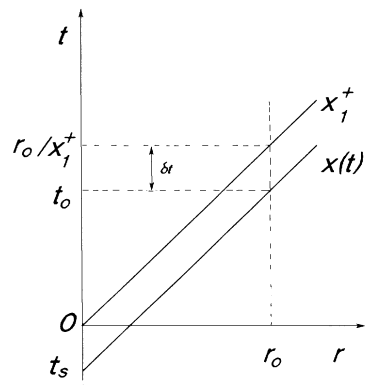

FIG. 19. A schematic space-time diagram for the redshift calculations. r_0 is the world line of the observer, while $r=0$ ($t<0$) is that of the source.

$$\delta x(t)=A\left[\frac{t}{t_s}\right]^{\bar{G}}, \tag{5.14}$$

where A does not depend on t_s. As t_s approaches 0,

$$\delta x(t_0)\approx A\left[\frac{r_0}{x_1^+|t_s|}\right]^{\bar{G}}. \tag{5.15}$$

We define

$$\delta t\equiv t_0-\frac{r_0}{x_1^+}=r_0\left[\frac{1}{x(t_0)}-\frac{1}{x_1^+}\right]. \tag{5.16}$$

Since $\delta x\to 0$,

$$\delta t=-r_0\delta\left[\frac{1}{x}\right]\simeq r_0\frac{\delta x}{x_1^{+2}}. \tag{5.17}$$

Using Eqs. (5.15) and (5.17) we obtain

$$\delta t\approx-\frac{r_0}{(x_1^+)^2}A\left[\frac{r_0}{x_1^+|t_s|}\right]^{\bar{G}} \tag{5.18}$$

and

$$\frac{d\delta t}{dt_s}=\frac{\bar{G}A}{x_1^+}\left[\frac{r_0}{x_1^+|t_s|}\right]^{\bar{G}+1}. \tag{5.19}$$

Substitution of (5.19) in (5.9) yields

$$z\approx\frac{A\bar{G}}{x_1^+}\sqrt{g_{tt}(x_1^+)}\left[\frac{r_0}{x_1^+|t_s|}\right]^{\bar{G}+1}. \tag{5.20}$$

Finally we use the definition of $\bar{G}$ [Eq. (5.12)] and Eq. (5.7) to obtain

$$\bar{G}+1=\left[\frac{d}{dx}e^{(\nu-\lambda)/2}\right]\Big|_{x=x_1^+}=\frac{1}{2}x\left[\frac{d(\nu-\lambda)}{dx}\right]\Big|_{x=x_1^+} \tag{5.21}$$

which, using Eqs. (2.9a) and (2.9b) becomes

$$\bar{G}+1=e^{\lambda}[2m-(1-k)D]. \tag{5.22}$$

In the Newtonian limit $k\to 0$ we have $\bar{G}+1=k\bar{D}_\infty$. In all the cases that we have examined numerically $0<\bar{G}+1<1$. Hence the redshift diverges like a power of t_s. Ori and Piran[15] have shown that the redshift diverges like a power law; however, the expression for the redshift given in Ref. 15 is wrong.

For asymptotically flat solutions with a cutoff (see Sec. VI) the redshift measured by an observer at infinity is obtained from Eq. (5.20), if one replaces r_0 by $r_c(x_1^+)$ and multiplies the RHS by the factor $[1-2m_b/r_c(x_1^+)]^{-1/2}$. Here, $r_c(t)$ [or $r_c(x)$] is the world line of the cutoff, and m_b is the total mass of the collapsing object.

H. Nonradial simple null geodesics

In addition to the two simple RNG's x_1^+ and x_2^+ there is a nonradial simple null geodesics from the singularity at (0,0) to infinity. Since our space is spherical we can consider such a geodesic in the equatorial plane ($\theta=\pi/2$) without any loss of generality.

There are three nontrivial geodesic equations:

$$\frac{dk_\phi}{d\lambda}=0 \tag{5.23a}$$

which yields $k_\phi=\text{const}\equiv -L$,

$$\frac{dk_t}{d\lambda}-\frac{1}{2}\frac{\partial g_{rr}}{\partial t}k^{r2}-\frac{1}{2}\frac{\partial g_{tt}}{\partial t}k^{t2}=0, \tag{5.23b}$$

and

$$g_{rr}k^{r2}+g_{tt}k^{t2}+g_{\phi\phi}k^{\phi 2}=0, \tag{5.23c}$$

where $k^\alpha=dx^\alpha/d\lambda$ and λ is an affine parameter. The condition that the geodesic is simple: $r=x_l t$ yields

$$k^{t2}(x_l^2g_{rr}+g_{tt})=-\frac{L^2}{r^2}=-\frac{L^2}{x_l^2}\frac{1}{t^2}. \tag{5.24}$$

We define

$$h(x)\equiv g_{rr}(x)+g_{tt}(x)/x^2 \tag{5.25}$$

and obtain, from Eq. (5.24),

$$k^{t2}=-\frac{L^2}{x_l^2h(x_l)}\frac{1}{t^2}. \tag{5.26}$$

If $h(x_l)<0$, Eq. (5.26) has a solution

$$\lambda=\frac{x_l^2\sqrt{-h(x_l)}}{2L}t^2, \tag{5.27'}$$

where we have chosen an integration constant such that $\lambda=0$ at (0,0). We can rescale λ to obtain

$$\lambda=t^2 \tag{5.27}$$

in which case

$$L=\frac{x_l^2}{2}\sqrt{-h(x_l)}. \tag{5.28}$$

Substitution of Eqs. (5.27) and (5.26) in (5.23b) yields

$$\frac{x_l^2}{2}(g'_{rr}+g'_{tt}/x_l^2)=g_{tt} \tag{5.29}$$

which is equivalent to $h'(x_l)=0$. We have found that a simple nonradial null geodesic of the form

$$t=\sqrt{\lambda},\quad r=x_l t,\quad \phi=\phi_0+\sqrt{-h(x_l)}\ln t\ , \tag{5.30}$$

exists if $h'(x_l)=0$, $h(x_l)<0$. This geodesic spirals outward, with r increasing by a factor of $\exp[2\pi/\sqrt{-h(x_l)}]$ every rotation in ϕ.

g_{tt}/x^2 vanishes for both $x=\infty$ and $x=0^+$. Hence $h=g_{rr}>0$ at these points. It follows from Eq. (5.25) that h vanishes only at the simple RNG's. Therefore, if there are no simple outgoing RNG's $h>0$ for $t>0$ and there is no simple outgoing spiral null geodesic. If the (0,0) singularity is naked, h vanishes and changes its sign at both x_1^+ and x_2^+. h has a minimal value at $x_l(x_1^+<x_l<x_2^+)$. Clearly $h(x_l)<0$ and $h'(x_l)=0$ and there is a simple outgoing spiral null geodesic at x_l.

As the radial simple null geodesics, the spiral simple null geodesic is tangent to a homothetic Killing vector. This vector field is a linear combination of the radial homothetic Killing field and the azimuthal Killing field $d\phi$.

I. The strength of the singularity

An interesting feature is the strength of the singularity at (0,0). Lake[22] and Waugh and Lake[18] have shown that the null geodesics x_1^+ emerges from a strong singularity. We extend here, his arguments to all simple null geodesics that either emerge from or terminate at the singularity at (0,0).

Clarke and Królak[34] have shown that a sufficient condition for strong singularity as defined by Tipler[17] is that at least one null geodesics, with an affine parameter λ, ends at the singularity at λ_s with

$$\lim_{\lambda\to\lambda_s}\lambda^2 R_{\alpha\beta}k^\alpha k^\beta\neq 0\ . \tag{5.31}$$

Equation (5.31) means that the limit exists and that it does not vanish. For a perfect fluid,

$$R_{\alpha\beta}k^\alpha k^\beta=8\pi[(p+\rho)u_\alpha u_\beta]k^\alpha k^\beta\ . \tag{5.32}$$

We consider now a simple null geodesics at $R=y_0T$ (corresponding to $r=x_0t$). In SSC coordinates the RHS of Eq. (5.32) becomes

$$R_{\alpha\beta}k^\alpha k^\beta=8\pi(k+1)\rho g_{TT}k^{T2}$$
$$=(k+1)\left[\frac{2D(y_0)g_{TT}(y_0)}{\bar r^{\,2}(y_0)}\right]\frac{1}{T^2}\left[\frac{dT}{d\lambda}\right]^2\ . \tag{5.33}$$

The term $[D(y_0)g_{TT}(y_0)\bar r^{\,2}(y_0)]$ is constant along y_0. Using Eq. (5.33) we find that the condition for a strong singularity becomes

$$\lim_{\lambda\to 0}\frac{\lambda^2}{T^2}\left[\frac{dT}{d\lambda}\right]^2\neq 0\ , \tag{5.34}$$

where we have chosen $\lambda_s=0$. We transform now to SSS coordinates and use the relations $r=x_0t=\bar r(y_0)T$ to rewrite Eq. (5.34) as

$$\lim_{\lambda\to 0}\frac{\lambda^2}{t^2}\left[\frac{dt}{d\lambda}\right]^2\neq 0\ . \tag{5.35}$$

We have seen earlier [Eq. (5.30)] that the spiraling simple null geodesic at x_l satisfies $t=\lambda^{1/2}$. The equation of motion of the radial simple geodesics,

$$\frac{dk_t}{d\lambda}-\frac{1}{2}\frac{\partial g_{rr}}{\partial t}k^{r2}-\frac{1}{2}\frac{\partial g_{tt}}{\partial t}k^{t2}=0\ , \tag{5.36}$$

yields

$$g_{tt}\frac{d^2t}{d\lambda^2}+\frac{x_0}{2}(x_0^2g'_{rr}+g'_{tt})\frac{1}{t}\left[\frac{\partial t}{\partial\lambda}\right]^2=0\ . \tag{5.37}$$

Hence $t=\lambda^\epsilon$ where

$$\epsilon=\frac{g_{tt}}{g_{tt}+\frac{x_0}{2}(x_0^2g^1_{rr}+g^1_{tt})}\ . \tag{5.38}$$

Using the function h, that we have defined in Eq. (5.25) we rewrite ϵ as

$$\epsilon^{-1}=2+\frac{x_0^2}{2g_{tt}(x_0)}x_0h'(x_0) \tag{5.39}$$

$xh'>0$ for x^- and x_1^+, $xh'=0$ for x_l, and $xh'<0$ for x_2^+. Hence, $\epsilon>\frac{1}{2}$ for x^-, x_1^+, $\epsilon=\frac{1}{2}$ for x_l, and $\epsilon<\frac{1}{2}$ for x_2^+. In all cases $\lim_{x\to 0}(\lambda^2/t^2)dt/d\lambda=\epsilon^2\neq 0$. Clearly the singularity is strong.

VI. MATCHING TO AN ASYMPTOTICALLY FLAT REGION

A. The cutoff

The self-similar solutions that we have described so far are not asymptotically flat. It follows directly from the self-similar structure that $\lim_{x\to\infty}m/r=M_\infty\neq 0$. Consequently, the total mass diverges and $\lim_{r\to\infty}g_{rr}\neq 1$ and $\lim_{r\to\infty}g_{tt}\neq -1$. To obtain an asymptotically flat spacetime we must limit the self-similar solution to a finite interior and match it to an asymptotically flat solution. We have seen earlier that some self-similar solutions contain naked singularities. We show in this section that we can introduce a cutoff in such a way that the local solution near the singularity remains unchanged and the singularity remains naked.

We introduce the cutoff to the initial values (on some spacelike hypersurface) in such a way that the density is the self-similar density for $0\le r\le r_i^0$. The density decreases smoothly to zero in the range $r_i^0\le r\le r_e^0$ and it vanishes identically for $r>r_e^0$ (see Fig. 20). Clearly the total mass with this profile is finite.

The cutoff perturbs the self-similar solution. The internal front of the perturbation moves inward along a world line $r_i(t)$. The solution is not self-similar for $r>r_i(t)$. The external perturbation front moves along another

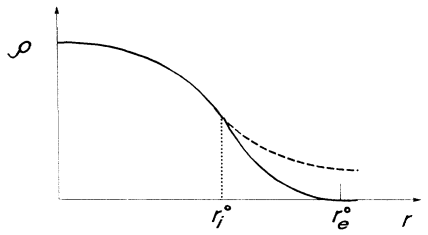

FIG. 20. An initial self-similar density profile with a cutoff at $r=r_i^0$. The density vanishes for $r>r_e^0$.

world line $r_e(t)$ and the space-time is empty for $r>r_e(t)$.

The internal perturbation front propagates inward as a rarefaction wave at the speed of sound. It is difficult to study analytically features of the expanding solution within the rarefaction wave region. But it is straightforward to study the motion of the rarefraction wave front $r_i(t)$. An incoming radial curve that moves at the speed of sound a_s satisfies

$$\frac{dR}{dT}=-a_s\left[\frac{-g_{TT}}{g_{RR}}\right]^{1/2}. \tag{6.1}$$

This equation resembles Eq. (5.1) and the space of solutions is also quite similar. There is one simple solution, satisfying $R=Y_{\rm sp}T$, at the sonic point. In addition there are two equivalence classes of curved solutions. Solutions interior to $Y_{\rm sp}$ reach the origin at $T<0$. The solutions exterior to $Y_{\rm sp}$ reach the origin at $T>0$. Let $r_{\rm sp}$ be the location of the sonic point on the initial slice. If the initial cutoff point satisfies $r_i^0>r_{\rm sp}$, then $r_i(t)$ will reach the origin only after the singularity forms at the origin. In such a case the cutoff will not influence the structure of the singularity and its nearby region.

Common hydrodynamic considerations suggest that the rarefaction wave moves inward at the speed of sound. Even if the perturbation is supersonic, its speed is bounded by the speed of light. If we choose $r_i^0>r^-=x^-t$, the ingoing null rays that leave r_i^0 will reach $r=0$ at $T>0$, and the region near the singularity will not be influenced by the cutoff.

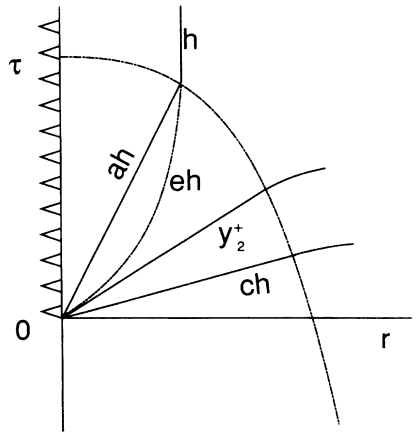

FIG. 21. The influence of a cutoff on the causal structure of a solution with a naked singularity. h is the absolute horizon (in the vacuum region), and eh is the event horizon (in the self-similar region).

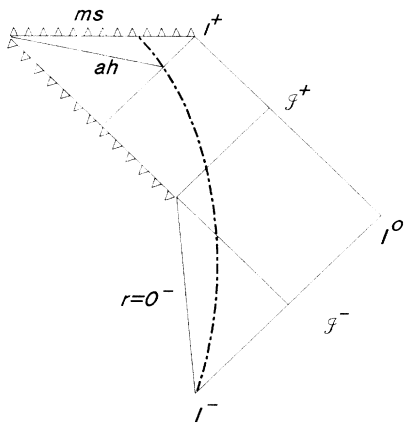

FIG. 22. Penrose diagram of the naked-singularity solution with a cutoff. This diagram ignores the mass of the shell at $r_c(t)$. The effect of this massive shell is to introduce a discontinuity in the apparent horizon (at its intersection with the cutoff line).

B. Global structure in a space-time with a cutoff

From the discussion in the previous section it is clear that (for a proper choice of initial cutoff) the local properties of the (0,0) singularity are unchanged by the cutoff. It is still possible, however, that the *global* structure is changed. It is, therefore, important to study the behavior of null geodesics in the matched space-time.

In order to visualize the behavior of geodesics in the whole space-time we introduce here the "sharp cutoff approximation" according to which the intermediate region "shrinks" to the "effective cutoff" curve $r\equiv r_c(t)$. For $r<r_c(t)$ the solution is self-similar, and for $r>r_c(t)$ it is Schwarzschild. This matching requires a thin massive

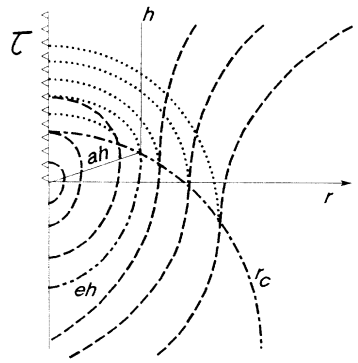

FIG. 23. Schematic description of outgoing RNG's in a solution without a naked singularity and with a cutoff. The dotted lines denote the shape of the RNG's in a solution without a cutoff. For more details see the caption of Fig. 21.

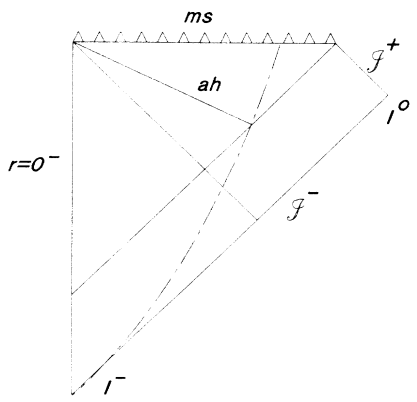

FIG. 24. Penrose diagram of solutions without a naked singularity and with a cutoff (see Fig. 22).

shell at $r_c(t)$, whose mass and tension depend on $r_c(t)$ (Ref. 35). This approximation is only for visualization purposes and the global causal structure does not depend on it. We choose the location of the cutoff in such a way that the singular center (0,0) is not in the causal feature of r_c^0. We distinguish between space-time with and without a naked singularity.

Naked singularity case. The overall behavior of the incoming RNG's is not influenced by the cutoff. Figure 21 describes the influence of the cutoff on the outgoing RNG's. All the outgoing RNG's that emerge before y_2^+ reach the cutoff line and continue from there to null infinity as regular radial geodesics in the Schwarzschild metric (at $r>2m$). y_1^+ remains the Cauchy horizon of the space-time. In the complete self-similar space-time all the geodesics that emerge after y_2^+ fall back into the massive singularity. With the cutoff some of those RNG's escape to null infinity. Hence, with the cutoff, y_2^+ is no longer the event horizon. The event horizon is the RNG that meets the apparent horizon at $r_c(t)$ (see Fig. 21). Figure 22 displays the Penrose diagram for these solutions (see Fig. 16 for comparison with the Penrose diagram of the fully self-similar solution).

This causal structure does not depend crucially on the sharp cutoff approximation. One can always choose the initial slice in such a way that, independently of the assumptions about the evolution of the "tail," the (0,0) singularity is *globally* naked. We demonstrate that in Appendix B.

Solutions without a naked singularity. Figure 23 describes the outgoing RNG's in these solutions. The outgoing RNG's that reach $r_c(t)$ before ah escapes to null infinity. All the others are trapped and fall back into the singularity. Figure 24 displays the Penrose diagram for these solutions. Here, due to the cutoff, some outgoing RNG's reach future null infinity. This future null infinity did not exist in the complete self-similar solution (see Fig. 17).

VII. THE SONIC POINT

A. Local behavior

The sonic point x_{sp} is the point where the magnitude of the fluid velocity V_F relative to the similarity lines,

$$V_F=\frac{\left[\frac{u^r}{u^t}-x\right]\left[-\frac{g_{rr}}{g_{tt}}\right]^{1/2}}{1-x\frac{u^r}{u^t}\left[-\frac{g_{rr}}{g_{tt}}\right]}=y\left[-\frac{g_{RR}}{g_{TT}}\right]^{1/2}, \tag{7.1}$$

is equal to the speed of sound $a_s=\sqrt{k}$. V_F vanishes at the regular center and diverges at $T=0$ ($y=\infty$) [see Eqs. (4.4) and (4.5)]; hence, there must be at least one sonic point in the solution.

The world line $r=x_{sp}\cdot t$ is both a characteristic line and a similarity line. Hence, the solution in the domain $|x|<|x_{sp}|$ does not determine the solution in the domain $|x|>|x_{sp}|$. Equations (2.9a)–(2.9d) can be expressed formally as

$$\mathcal{A}\frac{d\bar{p}}{dx}+\bar{B}=0\ , \tag{7.2a}$$

where

$$\bar{p}=\begin{bmatrix} D \\ u^r \\ \mathcal{M} \end{bmatrix} \tag{7.2b}$$

is a three-dimensional vector, $\mathcal{A}$ is a 3×3 matrix, and $\bar{B}$ is a three-dimensional vector. $|\mathcal{A}|$ vanishes when $V_F=\pm a_s$. Hence, at $x=x_{sp}$ the derivatives $d\bar{p}_i/dx$ either diverge or are undetermined. In the first case, it is impossible to extend the self-similar solution beyond $x=x_{sp}$ continuously. We will consider here only the latter case where x_{sp} is a critical point.

Bogoyavlensky[11] and Bicknell and Henriksen[13] have studied the local behavior of the solutions near x_{sp}. We show, here, how the sonic point influences the structure of the space of solutions. (Bicknell and Henriksen[13] have investigated the space of cosmological solutions which are asymptotically Friedmann without a regular center. We focus here on collapse solutions, with a regular center.) We first describe the basic features of the local behavior near x_{sp}. In this discussion we follow Bicknell and Henriksen.[13]

Consider the 3×4 matrix $\hat{\mathcal{A}}$, defined by

$$\hat{\mathcal{A}}_{ij}=\mathcal{A}_{ij},\quad \hat{\mathcal{A}}_{0j}=B_j\ , \tag{7.3}$$

where $i,j=1,3$ throughout this section. In order that x_{sp} will be a critical point [i.e, in order that Eq. (7.2) will have a finite solution] the rows of $\hat{\mathcal{A}}$ must be linearly dependent. One can show that this requirement is satisfied if

$$q\equiv(k+Y)^2-k(1-Y)^2+2kY(2Y-1/D)=0\ . \tag{7.4}$$

The equation $|\mathcal{A}|=0$ (or $V_F=a_s$) defines a two-dimensional surface in the three-dimensional space of physical variables $(D,u^r,\mathcal{M})$. This surface S_p is the locus

of all possible sonic points. The additional requirement $q=0$ define a one-dimensional curve C_p on S_p. All the (acceptable) solutions must cross S_p at C_p. We need a single parameter to specify the points of C_p. A convenient choice is $Y=\mathcal{M}/D$.

We define the four-dimensional vector

$$\hat{p} \equiv \begin{bmatrix} x \\ \bar{p} \end{bmatrix} . \tag{7.5}$$

Equation (7.2) now becomes

$$\hat{\mathcal{A}}\, d\hat{p}=0 . \tag{7.6}$$

Generally (for $x \neq x_{sp}$) this equation has a one-dimensional space of solutions, equivalent to well-defined dp_i/dx values. On C_p the linear dependence of the rows of $\hat{\mathcal{A}}$, results in a two-dimensional space of solutions of Eq. (7.6) (corresponding to a one-parameter family of dp_i/dx values).

To study the local behavior of solutions near a critical point $\hat{p}_0$, one can expand Eq. (7.2) [or Eq. (7.6)] to first order in $\delta\hat{p} \equiv \hat{p}-\hat{p}_0$. The general solution of the linearized equations can be expressed in the parametric form

$$\delta\hat{p}=a_1\hat{V}_1\eta^{\lambda_1}+a_2\hat{V}_2\eta^{\lambda_2} , \tag{7.7}$$

where η is an arbitrary parameter, a_1 and a_2 are arbitrary constants, and λ_1,λ_2 are two (generally nonzero) eigenvalues of a 4×4 matrix, constructed from the various derivatives of elements of $\hat{\mathcal{A}}$ at $\hat{p}_0$. $\hat{V}_1$ and $\hat{V}_2$ are the two corresponding eigenvectors of that matrix. λ_1, λ_2, $\hat{V}_1$, and $\hat{V}_2$ (but not a_1,a_2) are determined by $\hat{p}_0$. It is possible to rescale the parameter η and with this to change the values of a_1 and a_2 without changing the solution. Hence, Eq. (7.7) describes only a one-parameter family of solutions.

The critical points are divided into two principle types.

(1) A saddle point: $\lambda_1/\lambda_2<0$. Two distinct solutions cross each such critical point, in the "directions" V_1 and V_2 correspondingly. Both solutions are analytic at x_{sp}.

(2) A nodal point: $\lambda_1/\lambda_2>0$. As before, there are two analytic solutions that cross at x_{sp}, in the directions V_1 and V_2. In addition, there is a one-parameter set of solutions in the range $x<x_{sp}$ that terminate at x_{sp}, and an equivalent one-parameter set in the range $x>x_{sp}$. At x_{sp} both one-parameter sets are nonanalytic and tangent to V_1. By combining a solution in $x<x_{sp}$ with one in $x>x_{sp}$, one finds that a two-parameter set of (nonanalytic) solutions pass x_{sp} in the direction V_1. V_1 is called, therefore, the "principle direction" and V_2 is the secondary one. In this sense, a nodal point is "attractive."

Most of the self-similar solutions (except of a set of "measure zero") pass a nodal critical point, as primary-direction solutions, in a nonanalytic manner. All the GRPL solutions pass a nodal point (analytically) in the secondary direction. The homogeneous solutions also pass a nodal point analytically, in the primary direction for $k<\frac{1}{3}$ and in a secondary direction for $k>\frac{1}{3}$.

The critical point is a node for $\epsilon>0$ and a saddle for $\epsilon<0$, where

$$\epsilon \equiv \frac{1+k+\sqrt{c}}{1+k-\sqrt{c}} \tag{7.8}$$

and $c=(4+12k)Y^2+(1+6k-3k^2)(1-4Y)$. In both cases c is positive.

There are sections of C_p where c is negative. In this case ϵ is complex and x_{sp} is a "focal point," with the mathematical solution spiral around x_{sp}. However, such a spiraling solution is physically meaningless, and physical solutions cannot reach a focal point. In the limiting case $c=0$ ($\epsilon=1$) x_{sp} is called "a degenerate node." The behavior is quite similar to a nodal point, except that now V_1 coincides with V_2 (see, e.g., Ref. 16).

We note that the discussion here refers only to the local behavior near x_{sp}. Additional requirements (such as the existence of regular center) will further reduce the space of solutions.

B. Implication to the space of solutions

We now turn to study the way the critical point influences the space of self-similar solutions. An acceptable solution is one which is regular both at the center and at the sonic point. In Sec. II we have shown that (for a given k) there is a one-parameter family of solutions with a regular center (parametrized by D_0). A numerical study shows that the space of solutions has a band structure (see Fig. 25): The D_0 axis is divided into "allowed" ranges and "forbidden" ranges (for which the solution terminates at the sonic point). In every band, most of the solutions approach a nodal critical point, as nonanalytic primary-direction solutions. This behavior is due to the "attractive" nature of the nodal critical points. In every band the parameter D_0 determines the solution up to x_{sp}. However, since an infinite number of solutions in the range $|x|>|x_{sp}|$ terminate at every nodal point an additional parameter is required to determine the solution beyond x_{sp}. Every band is therefore a one-parameter

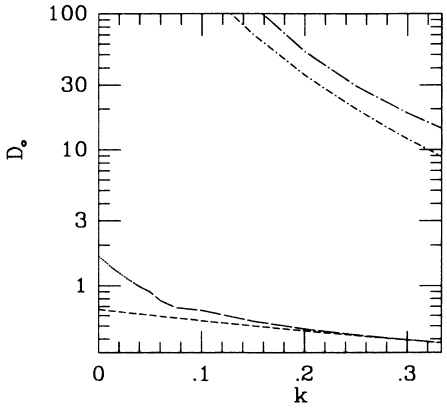

FIG. 25. The first two bands in the D_0-k plane. The first band lies below the dotted–long-dashed lines. The second band is located between the two dashed-dotted lines. The short-dashed line is the homogeneous solution, and the dotted line is the GRPL solution.

family at $|x|<|x_{sp}|$, and a two-parameter family at $|x|>x_{sp}|$. Since the space of self-similar solutions is two dimensional (for a given k), we conclude that beyond x_{sp} the subset of centrally regular solutions is "of nonzero measure" in the global space of self-similar solutions.

The requirement of analyticity at the sonic point reduces drastically the space of solutions. In every band there are only a few (generally one or two) D_0 values for which the solution approaches x_{sp} analytically. Once the critical point is approached analytically, there is only one analytic way to continue the solution beyond it. Hence, those special solutions span only a discrete set (for a given k).

Figure 25 presents the first two bands in the D_0-k plane. The first band is below the line which consists of the GRPL line (for $k<0.036$) and the short-dashed line (for $k>0.036$). This short-dashed line represents a solution with a "degenerate node." For $k>\frac{1}{3}$ (not shown in Fig. 25) the upper boundary is the homogeneous solution. The GRPL solutions and the homogeneous solutions are the only analytic (at x_{sp}) solutions in this band.

The upper boundary of the second band has a similar structure to the upper boundary of the first band (for $k<\frac{1}{3}$): degenerate node solutions for $k>0.11$ and secondary direction nodal-point solutions (such as the GRPL solutions) for $k<0.11$ (not shown in Fig. 25). The lower boundary contains solutions with a saddle point. These are "bouncing solutions" (see Sec. IV), and those with $k>0.25$ are "exploding solutions."

It is likely that the structure of the higher bands is similar to the structure of the second one (apart from the number of "wiggles"). Saddle-point, bouncing (and exploding), solutions are the lower boundary. The upper boundary contains either secondary-direction nodal-point solutions, or degenerate-node solutions. All the solutions in the interior of these bands pass through a nodal point in the primary direction.

C. The kink instability

The existence of a sonic point in the solutions raise the question of stability to appearance of a shock there. Ori and Piran[19] have studied, analytically, the dynamics of a discontinuity in the first derivatives of the velocity and the density at the sonic point, in the framework of the Newtonian model. They have shown that all secondary direction solutions are stable to this perturbation, but the primary directions are not. This instability results in either a development of a different stable profile or in a divergence of V' and D' (which probably indicates an appearance of a shock wave). It implies that all the nonanalytic solutions (which are all primary direction) and the homogeneous collapse solution are unstable in this sense.

One can show that the kink instability exists also in the relativistic model. In Sec. III we have shown that all the relativistic solutions become approximately Newtonian at the limit $k\to 0$. Therefore, we expect that at least for small enough k values, only secondary direction solutions can be stable.

D. The sonic point and the initial-value problem

As was stated earlier, the sonic point introduces an ambiguity in the self-similarity equations. Some solutions terminate there, that is, there is no smooth self-similar continuation beyond the sonic point. For other solutions there are many such continuations. It is therefore important to note that no such ambiguity exists in the field equations themselves. For, if a self-similar solution terminates at x_{sp}, one cannot build from it a self-similar initial slice. Or, if there are many possible continuations beyond x_{sp}, then a given self-similar initial slice will conform with one of them. Indeed, this specific continuation will govern the evolution of the system in the future.

On the other hand, in some of the solutions there is a second sonic point at $T>0$. Although the mathematical behavior of the self-similar equations there is similar to the $T<0$ sonic point, there is a fundamental difference from the causal point of view. Here, the initial slice (at $T<0$) does not contain the information about the continuation. In consequence the ambiguity in the continuation of the self-similar solution represents a true ambiguity in the evolution. However, this ambiguity is not surprising, because the $T>0$ sonic point is always located to the future of the Cauchy horizon.

VIII. SELF-SIMILAR DUST SOLUTIONS

The self-similar dust ($k=0$) case is a special case of the well-known Tolman-Bondi solution. To compare it with our formalism we use comoving coordinates (R,T). We scale the time coordinate such that T is the proper time ($g_{TT}=1$) and we scale R so that $R=m$ (both scalings are possible only in the dust case). The Tolman-Bondi solution is given by

$$g_{RR}=\frac{r'^2}{F(R)},\quad g_{TT}=-1,\quad \rho=\frac{1}{8\pi r^2 r'}\ , \tag{8.1}$$

where a prime denotes a derivative with respect to R, F is an arbitary function of R, and r the area coordinate is given, in the $F=0$ case, by

$$r=(\tfrac{9}{2}R)^{1/3}[T_0(R)-T]^{2/3} \tag{8.2}$$

and in the $F\neq 0$ case, by the parametric form

$$\begin{aligned} &r=\frac{R}{F}(\cosh\eta-1)\ ,\\ &T_0(R)-T=\frac{R}{F^{3/2}}(\sinh\eta-\eta)\quad \text{for } F>0\ , \end{aligned} \tag{8.3a}$$

$$\begin{aligned} &r=\frac{R}{-F}(1-\cos\eta)\ ,\\ &T_0(R)-T=\frac{R}{(-F)^{3/2}}(\eta-\sin\eta)\quad \text{for } F<0\ . \end{aligned} \tag{8.3b}$$

Here $T_0(R)$ is a second arbitrary function of R. T_0 is the time when the shell R crunches into the $r=0$ singularity. This solution is valid in the range $T<T_0(R)$.

In order to construct the self-similar solutions for Eqs. (8.1)–(8.3) we use the fact that in self-similar solutions every dimensionless quantity is a function of $y=R/T$

only. On the other hand, the dimensionless quantities F and T_0/R depend on R alone. Hence, we have in the self-similar case

$$F(R)=\text{const}, \quad \theta(R)\equiv\frac{T_0(R)}{R}=\text{const} . \tag{8.4}$$

One can show that Eq. (8.4) is also a sufficient condition for self-similarity. This solution is limited to the range $1/y<\theta$. As in the $k>0$ case, the space of self-similar $k=0$ solutions is two dimensional. Each solution is characterized by F and θ.

All the solutions with $F\neq 0$ do not have a regular center. To show this we consider the behavior at $r=0$ for $T\neq 0$. According to Eqs. (8.3a), (8.3b), and (8.4), $T\neq 0$ implies $m=R\neq 0$. Thus, instead of a regular center there is a massive singularity at $r=0$. One can easily check using Eq. (8.1) that ρ and u^r also diverge there. Hence, the family of solutions with a regular center is only a one-parameter family. In the $k>0$ case, because of the regularity requirement the space of solutions for $|x|<|x_{\rm sp}|$ is one dimensional. But the space of solutions is two dimensional beyond $x_{\rm sp}$ (due to the branching at the sonic point). In the dust case $a_s=0$ and there is no sonic point.

We shall consider only the case $F=0$, for which we have

$$r=(\tfrac{9}{2}R)^{1/3}(\theta R-T)^{2/3} , \tag{8.5}$$

$$\rho=\frac{1}{4\pi r' r^2}, \quad g_{RR}=r'^2, \quad g_{TT}=-1 . \tag{8.6}$$

One can obtain from Eqs. (8.5) and (8.6) an explicit expression for ρ:

$$\rho=\frac{1}{12\pi}[(\theta R-T)(3\theta R-T)]^{-1} . \tag{8.7}$$

Using Eqs. (8.5) and (8.7), we expand $\rho(r,T)$ near the regular center, for a given $T<0$, as a power series of r:

$$\rho=\frac{T^2}{12\pi}\left[1+\frac{a_3}{T_3}r^3+\frac{a_6}{T^6}r^6+\cdots\right] \tag{8.8}$$

(a similar expansion but with r and t instead of r and T will have a similar form). Analyticity at $R=0$ requires an expansion of the form $\rho=a_0(T)+a_2(T)r^2+a_4(T)r^4+\cdots$. Hence, even the $F=0$ self-similar dust solutions are not analytic (though not singular) at $r=0$, $T<0$ (Ref. 36). These solutions were not included among the Tolman-Bondi solutions studied by Christodoulou[7] and Newman.[20] Unlike the dust solutions, all the $k>0$ solutions considered earlier are analytic at $r=0$ [see Eq. (2.15a)].

We turn now to study the causal structure of the dust solutions. In Sec. V we have shown that a necessary and sufficient condition for a naked singularity at $R=T=0$ is the existence of a simple outgoing RNG: $R=y^+t$. Such a RNG, if it exists, must satisfy $0<y^+$ and $\theta>1/y^+$. Hence θ must be positive. $R=y^+t$ is a RNG if $y^{+2}g_{RR}=1$. According to Eq. (8.6) this reads

$$T/R=r'=\tfrac{1}{3}(\tfrac{9}{2})^{1/3}[(\theta-T/R)^{2/3}+2\theta(\theta-T/R)^{-1/3}] . \tag{8.9}$$

Defining $z=(\theta-T/R)^{1/3}$, Eq. (8.9) is reduced to

$$z^4+6^{-1/3}z^3-\theta z+2\times 6^{-1/3}\theta=0 \tag{8.10}$$

with the constraint $0<z<\theta$. A solution of Eq. (8.10) exists for $\theta>\theta_c\equiv\frac{26}{3}+5\sqrt{3}$ (Ref. 37). Hence, all the solutions with $\theta>\theta_c$ have naked singularity.

As in the $k>0$ case, a self-similar dust solution which is locally naked, is also globally naked, and vice versa. This is in a remarkable contrast to the behavior of non-self-similar dust solutions which are analytic at $r=0$ ($T<0$). Those solutions are locally naked,[5,7,20] but might be globally dressed.[38]

Newman[20] has studied the strength of singularities in Tolman-Bondi solutions with analytic behavior at $r=0$, $T<0$. He found that all the naked singularities in these solutions are weak (in the sense of Tipler[17]). The assumption of analytic behavior at $r=0$, $t<0$ is critical in his analysis. In Sec. V we have shown that all naked singularities in the self-similar solutions are strong. Clearly, this analysis includes the $k=0$ case as well (see, also, Ref. 18).

So far we have obtained the self-similar dust solution as a special case of the Tolman-Bondi solutions. One can also obtain the self-similar dust solutions from the $k>0$ solutions by letting k approach to zero, with fixed D_T and u^r_T. (We recall that the Newtonian solutions are obtained also by a $k\to 0$ limiting process, but with fixed $\bar{D}_T=D_T/k$ and $u^r_T/\sqrt{k}$.) The properties of the $k>0$ solutions can generally be translated to the dust case simply by substituting $k=0$ in the relevant expressions. Most properties of the $k>0$ solutions are invariant to this change: the existence of solutions with and without naked singularities, the existence of simple RNG's and their implications on the causal structure, the existence of a spiral RNG, the divergence of redshift along x^+_1, etc.

There are, however, a few differences. (1) In the limiting process $k\to 0$, $x_{\rm sp}$ tends to zero. Hence, all the oscillatory structure (which might exist for $k>0$ in the region $0<|x|<|x_{\rm sp}|$; see Sec. IV) does not exist in the dust case. Also, there is no band structure in the space of solutions. (2) As mentioned earlier, there is only one-dimensional family of solutions with regular center. Even those solutions are not analytic at $r=0$. (3) g_{TT} does not diverge at $T=0$. (4) The matching of a self-similar interior to a vacuum exterior is trivial.

ACKNOWLEDGMENTS

We would like to thank the Institute for Advanced Study in Princeton for hospitality while part of this research was done. This research was supported by a Grant from the US-Israel Binational Science Foundation to the Hebrew University.

APPENDIX A

Initially we have four equations [Eqs. (2.29a)–(2.29c)] for the four variables ν, λ, D, and u^r. We have eliminat-

ed ν between Eqs. (2.29a) and (2.29c) to obtain Eqs. (2.11)–(2.13). There remain now three equations [say, Eqs. (2.29b)–(2.29d)], for the three variables λ, D, and u^r. Equation (2.9b) can be written as

$$x\lambda' = A_0(\lambda, D, u^r) . \tag{A1}$$

In view of Eq. (2.12),

$$x\nu' = 2 + x\frac{d\ln[Q^2/(1+e^{\lambda}u^{r2})]}{dx} ,$$

so that Eq. (2.9c) takes the formal form

$$A_1 x\lambda' + B_1 x u'' + C_1 x D' + D_1 = 0 . \tag{A2}$$

We now multiply Eq. (2.9d) by x and substitute Eqs. (2.12) and (2.13) in it to get rid of ν and u^t. It also takes now the form

$$A_2 x\lambda' + B_2 x u'' + C_2 x D' + D_2 = 0 . \tag{A3}$$

The coefficients $A_1, B_1, C_1, A_2, B_2, C_2$ are functions of λ, u^r, and D only so that Eqs. (A1)–(A3) form an autonomous set of differential equations for λ, u^r, and D with respect to the independent variable $\ln x$. Dividing Eqs. (A2) and (A3) by Eq. (A1) we finally obtain a closed system of two equations that express $du^r/d\lambda$ and $dD/d\lambda$ in terms of λ, u^r, and D.

APPENDIX B

The "worst" assumption about the evolution of the tail (from the point of view of outgoing null geodesics) is that all its matter is located at $r_i(t)$, and that $r_i(t)$ moves inwardly with the speed of light. Let us denote by P the intersection of y_1^+ with the incoming RNG that emerges from the initial cutoff point r_i^0, and let r_p be the r value of p. Clearly a sufficient condition for the singularity to be globally naked is $2m_b/r_p < 1$.

One of the degrees of freedom that is involved in the choice of initial data is the embedding $T_0(R)$ of the initial slice in the plane (R,T) of the self-similar solution. We require that $T_0(R)$ is spacelike and that the initial slice is regular. Regularity implies that for $R=0$ (the center), T_0 is negative. However, T_0 may increase with R (and may be positive for sufficiently high R values). In particular, one can choose $T_0(R)$ such that (for sufficiently high R values) it coincides with some similarity line $y=\text{const}\equiv y_0$ [i.e., $y_0 = R/T_0(R)$]. We define $\epsilon \equiv y_0 - y_1^+$ and for $\epsilon > 0$ one can always choose a spacelike curve $T_0(R)$ in that manner.

The total mass m_b consists of the self-similar part $r_i^0 \mathcal{M}(y_0)$ and the tail mass δ_m. In the limit ϵ, $\delta m \to 0$ we have $y_0 \to y_1^+$, $r_p \to r_i^0$, and $m_b \to r_i^0 \mathcal{M}(y_0)$. In this limit

$$\frac{2m_b}{r_p} \to \frac{2m_b}{r_i^0} \to 2\mathcal{M}(y_0) \to 2\mathcal{M}(y_1^+) < 1 .$$

Thus, one can always choose small enough ϵ and δ_m values such that the (0,0) singularity is globally naked.

*Electronic address: Tsvi@hujivms.

[1]J. R. Oppenheimer and H. Snyder, Phys. Rev. **56**, 455 (1939).
[2]R. Penrose, Riv. Nuovo Cimento **1**, 252 (1969).
[3]L. D. Landau and E. M. Lifshitz, *The Classical Theory of Fields*, 4th ed. (Course of Theoretical Physics, Vol. 2) (Pergamon, New York, 1975).
[4]P. Yodzis, H. J. Seifert, and H. Müller zum Hagen, Commun. Math. Phys. **34**, 135 (1973).
[5]D. M. Eardley and L. Smarr, Phys. Rev. D **19**, 2239 (1979).
[6]W. A. Hiscock, L. G. Williams, and D. M. Eardley, Phys. Rev. D **26**, 751 (1982).
[7]D. Christodoulou, Commun. Math. Phys. **93**, 171 (1984).
[8]K. P. Stanyukovich, O. Sharshekeev, and V. Ts. Gurovich, Dokl. Akad. Nauk SSSR **165**, 510 (1965) [Sov. Phys. Dokl. **10**, 1030 (1966)].
[9]M. E. Cahill and A. H. Taub, Commun. Math. Phys. **21**, 1 (1971).
[10]D. M. Eardley, Commun. Math. Phys. **37**, 287 (1974).
[11]O. I. Bogoyavlenskii, Zh. Eksp. Teor. Fiz. **73**, 1201 (1977) [Sov. Phys. JETP **46**, 633 (1977)].
[12]B. Carr and S. W. Hawking, Mon. Not. R. Astron. Soc. **168**, 399 (1974).
[13]G. V. Bicknell and R. N. Henriksen, Astrophys. J. **219**, 1043 (1978); **225**, 237 (1978).
[14]B. Carr and A. Yahil, report, 1988 (unpublished).
[15]A. Ori and T. Piran, Phys. Rev. Lett. **59**, 2137 (1987).
[16]A. Ori and T. Piran, Gen. Relativ. Gravit. **20**, 7 (1988).
[17]F. J. Tipler, C. J. S. Clarke, and G. F. R. Ellis, in *General Relativity and Gravitation*, edited by A. Held (Plenum, New York, 1980).
[18]B. Waugh and K. Lake, Phys. Rev. D **38**, 1315 (1988); **40**, 2137 (1989).
[19]A. Ori and T. Piran, Mon. Not. R. Astron. Soc. **234**, 821 (1988).
[20]R. P. A. C. Newman, Class. Quantum Grav. **3**, 527 (1986).
[21]K. Lake and C. Hellaby, Phys. Rev. D **24**, 3019 (1981); K. Lake, *ibid.* **26**, 518 (1982); B. Steinmuller, A. R. King, and P. J. Lasota, Phys. Lett. **51A**, 191 (1975).
[22]K. Lake, Phys. Rev. Lett. **60**, 241 (1988); K. Rajagopal and K. Lake, Phys. Rev. D **35**, 1531 (1987).
[23]M. V. Penston, Mon. Not. R. Astron. Soc. **144**, 449 (1969).
[24]R. B. Larson, Mon. Not. R. Astron. Soc. **145**, 271 (1969).
[25]F. H. Shu, Astrophys. J. **214**, 488 (1977).
[26]C. Hunter, Astrophys. J. **218**, 834 (1977).
[27]C. Hunter, Mon. Not. R. Astron. Soc. **223**, 391 (1986).
[28]A. Whitworth and D. Summers, Mon. Not. R. Astron. Soc. **214**, 1 (1985).
[29]A. Yahil, Astrophys. J. **265**, 1047 (1983).
[30]We show in Sec. IV that $\lim_{T\to 0} r(R,T) \neq 0$ for $R \neq 0$ and that D_{∞} is finite (in all solutions apart from a one-parameter family of solutions that we call "asymptotically Friedmann solutions").
[31]In Ref. 19 we show that all the primary-direction solutions are unstable. All the nonanalytic solutions and the homogeneous

solution are primary.

[32]We show in Sec. V that a black hole exists in solutions without a naked singularity only if we introduce a cutoff.

[33]In an asymptotically Friedmann solution there is a real singularity at $T=0$ and the asymptotic behavior is different.

[34]C. J. S. Clarke and A. Królak, J. Geom. Phys. **2**, 127 (1986).

[35]In particular one can choose $r_c(t)$ as a world line of some fluid shell.

[36]The only exception is the spatially flat Friedmann solution, for which $\theta=0$.

[37]D. M. Eardley, Phys. Rev. Lett. **33**, 442 (1974), discussed the time reversal of this problem.

[38]In the special case $a_2=0$ the singularity is always dressed, even locally.